The involvement of the transcription factor ATF7 in the regulation of metabolism

（代謝制御における転写因子 ATF7 の役割）

2017

筑波大学グローバル教育院
School of the Integrative and Global Majors in University of Tsukuba
Ph.D. Program in Human Biology
Yang Liu
劉　陽

筑波大学

University of Tsukuba

博　士（人間生物学）学　位　論　文

PhD dissertation in Human Biology

The involvement of the transcription factor ATF7 in the regulation of metabolism

（代謝制御における転写因子 ATF7 の役割）

2017

筑波大学グローバル教育院

School of the Integrative and Global Majors in University of Tsukuba
Ph.D. Program in Human Biology

Yang Liu

劉　陽

Abstract

Purpose: The growing epidemic of obesity poses serious health risks due to the development of obesity-associated diseases including type 2 diabetes, hypertension, heart diseases, and cancer. When energy intake consistently exceeds energy expenditure, excess calories are stored as triglycerides in white adipose tissue. By contrast, brown adipose tissue (BAT) and beige adipocytes are responsible for the dissipation of energy as heat by adaptive thermogenesis. The activating transcription factor (ATF)2 family of transcription factors regulates a variety of metabolic processes, including adipogenesis and adaptive thermogenesis. ATF7 is a member of the ATF2 family, and mediates epigenetic changes induced by environmental stresses, such as social isolation and pathogen infection. However, the metabolic role of ATF7 remains unknown. Assisted reproductive technologies, including in vitro fertilization (IVF), are now frequently used, and increasing evidence indicates that IVF causes gene expression changes in children and adolescents that increase the risk of metabolic diseases. Although such gene expression changes have been thought to be due to the IVF-induced epigenetic changes, its mechanism remains elusive. Thus I would like to investigate the role of ATF7 in regulation of metabolism and its function in the IVF-induced gene expression change.

Methods: To explore the role of ATF7 in metabolism, we measured a series of metabolic parameters of *Atf7*-deficient (*Atf7*$^{-/-}$) and wild type (WT) mice, including body weight, insulin and glucose tolerance, energy expenditure, plasma glucose,

triglycerides, and cholesterol concentrations, serum insulin and resistin levels. The histology analysis was performed to examine the cell morphology of adipose tissues. Gene expression changes were detected by RT-PCR and microarray analysis. Protein expression and phosphorylation level were examined by western blotting. In vitro differentiation was implemented for investigation of the role of ATF7 in adipogenesis. Bioinformatics methods were applied to analyze the gene expression pattern in liver.

Results: *Atf7*$^{-/-}$mice exhibited lower body weight and resisted diet-induced obesity. Serum triglycerides, resistin, and adipose tissue mass were all significantly lower in ATF7-deficient mice. Fasting glucose levels and glucose tolerance were unaltered, but systemic insulin sensitivity was increased by ablation of ATF7. Indirect calorimetry revealed that oxygen consumption by *Atf7*$^{-/-}$ mice was comparable to that of WT littermates on a standard chow diet, but increased energy expenditure was observed in *Atf7*$^{-/-}$mice on a high-fat diet. The thermogenic genes, including *Ucp1* and *Ppargc1a*, exhibited the higher expression levels in iWAT of *Atf7*$^{-/-}$ mice and the UCP1 expression level was higher in BAT of *Atf7*$^{-/-}$ mice after cold exposure. Adipogenesis was impaired by ablation of ATF7. In contrast, overexpression of ATF7 in C3H10T1/2 cells promoted the process of adipogenesis. We also found that IVF up-regulated the expression of 688 genes in the liver of 4-week-old wild-type (WT) mice, whereas 87% of these were not changed by IVF in *Atf7*$^{-/-}$ mice. The genes, which are involved in metabolism, such as pyrimidine and purine metabolism, were

up-regulated in WT mice but not in *Atf7*$^{-/-}$ mice. Of the genes whose expression was up-regulated by IVF in WT mice, 37% were also up-regulated by a loss of ATF7.

Conclusion: Our data showed that the ablation of ATF7 in mice could improve the resistance to diet-induced obesity and insulin sensitivity. *Atf7*$^{-/-}$ mice fed a HFD showed higher energy expenditure during both light and dark phases, implying that ATF7 may contribute to the regulation of adaptive thermogenesis. The up-regulated thermogenic genes in inguinal WAT of *Atf7*$^{-/-}$ mice and cold exposure-induced phosphorylation of ATF7 in BAT further confirm that ATF7 functions as transcriptional repressor in the thermogenic gene program. However, in vitro adipocyte differentiation demonstrated that ATF7 is required for adipogenesis. These data indicate that ATF7 controls the energy balance by regulation of adipocytes development and thermogenesis. In addition, our study also shown that ATF7 is a key factor in establishing the memory of IVF effects on metabolic pathways, such as pyrimidine and purine metabolism and terpenoid backbone biosynthesis.

Content

Introduction

1. ATF7 and the ATF2 transcription factor family

1.1 The ATF2 transcription factor family

The activating transcription factor (ATF)7 belongs to the ATF2 transcription factor family, which is a part of the ATF/cAMP response element-binding protein (CREB) superfamily. The vertebrate ATF2 family has three members: ATF2 (originally named CRE-BP1) [1,2], CRE-BPa[3], and ATF7 (originally named ATF-a)[4]. Each of these three proteins contains the DNA-binding domain involving a basic leucine zipper (B-ZIP) structure and a *trans*-activation domain consisting of a metal finger structure and stress-activated protein kinase (SAPK) phosphorylation sites. The B-ZIP DNA binding domains can bind to the cyclic AMP response element (CRE: 5'-TGACGTCA-3'). The SAPK phosphorylation sites on these proteins are the targets of SAPK p38[5] (Fig1-1, A).

The ATF2 family is conserved among various species. Atf1 is the *Schizosaccharomyces pombe* ortholog of the mammalian ATF2. In fission yeast, Atf1 is phosphorylated by the mitogen-activated protein kinase (MAPK) Sty1 in response to different stresses, including UV damage, nutritional starvation, nucleotide pool depletion, oxidative stress and osmotic stress[6]. Atf1 forms heterodimers with Pcr1 and these two proteins contribute to H3 lysine 9 methylation and Swi6-dependent heterochromatin formation[7]. The *Caenorhabditis elegans* ortholog, ATF7, also is one of targets of PMK-1 p38 MAPK pathway. It functions as the repressor of PMK-1–regulated immune effector gene expression in absence of stress. The

pathogen-induced activation of PMK-1 phosphorylates ATF7 and switches ATF-7 to an activator in order to induce the immune effector gene transcription[8]. dATF2 (also known as CG30420) is the ortholog of mammalian ATF2 and ATF7 in *Drosophila*, plays a critical role in the regulation of fat metabolism. dATF2 knockdown flies exhibit the reduced glyceroneogenesis and the smaller triglyceride reserves[9]. dATF2 in pacemaker neurons functions as a regulator of connection between sleep and locomotion. The knockdown of dATF2 decreases period of sleep time and increases locomotor activity of fly [10]. dATF2 contributes to the establishment of heterochromatin at early embryonic stage and the maintenance of heterochromatin during later stages. Various environmental stresses, including osmotic stress and heat shock, can induce phosphorylation of dATF2, leading to the release of dATF2 from chromatin and disruption of heterochromatin structure. Intriguingly, the dATF2 mediated stress-induced epigenome change can be inherited to the next generation in fly[11].

The molecular function of ATF2 is tightly controlled by protein modification, particularly by phosphorylation on Thr69 and Thr71, which is mediated by stress activated protein kinases p38 or JNK[6]. Several protein kinase C (PKC) isoforms can phosphorylate the ATF2 on Ser12 or Thr52, which enhances the nuclear retention of ATF2 and promotes its transcriptional activity[12]. In response to DNA damage induced by ionizing radiation (IR), ataxia-telangiectasia mutated (ATM) kinase phosphorylates ATF2 on Ser490 and 498, resulting in its localization into ionizing

radiation-induced foci and the recruitment of double-strand break repair protein MRE11A, indicating that ATF2 has the transcription-independent role[13].

ATF2 is ubiquitously expressed and the abundant expression of ATF2 was observed in the brain[14]. The ablation of *Atf2* gene in mice leads to postnatal lethality caused by meconium aspiration syndrome and severe respiratory defects[15,16]. ATF2 can form homodimer or heterodimer with members of the Jun, Fos or Maf transcription factor families to regulate a variety of cellular processes[17]. ATF2 exhibits oncogenic function within the nucleus. It associates with v-Jun to promote growth factor-independent proliferation in vitro and tumor formation in vivo[18]. ATF2 also acts as a tumor suppressor. ATF2 heterozygous mice are prone to develop mammary tumors due to the reduced expression of the mammary tumor suppressor gene *Maspin* and *Gadd45a*[19]. Besides, genotoxic stress can induce ATF2 localization at the mitochondria to increases mitochondrial permeability and promotes apoptosis[20].

In addition, ATF2 plays an essential role in the regulation of metabolism. By associating with β-cell-enriched transcription factors, MafA, Pdx1, and Beta2, ATF2 binds to the conserved CRE2 sequence of insulin promotor to enhance the transcription[21,22]. Using the $Atf2^{+/-}Cre\text{-}bpa^{+/-}$ double heterozygous mice, the function of ATF2 in the adipose tissue was investigated. The mutant mice exhibited reduced WAT mass and improved insulin sensitivity. ATF2 contributes to white adipocyte differentiation via p38-dependent induction of peroxisome proliferator-activated receptor (PPAR)γ2[23], which is a key transcription factor mediating adipocyte differentiation[24]. The p38-dependent phosphorylation of ATF2 is also involved in

thermogenic gene program. In response to cold exposure, ATF2 directly activates transcription of the UCP1 gene. This gene encodes uncoupling protein 1[25], which mediates non-shivering thermogenesis in brown adipose tissue (BAT)[26]. ATF2 also stimulates transcription of PPARγ coactivator-1α (PGC-1α) and zinc finger protein 516 (Zfp516), both of which also activate UCP1 transcription[27,28].

1.2 ATF7 functions as a transcriptional repressor

ATF7 shares a considerable conserved protein sequence to ATF2, particularly within the C-terminal B-ZIP DNA-binding domain and the N-terminal trans-activation domain (Fig. 1-1, A). The conserved threonine residues Thr51 and Thr53 in ATF7 (corresponding to the Thr69 and Thr71 in ATF2) are phosphorylated by MAPK, especially by p38 and Jun[29]. When ATF2 is phosphorylated by SAPKs in response to stimuli, it binds with its coactivator CREB-binding protein (CBP) and activates transcription[30]. ATF7 represses rather than activates gene transcription in the absence of stress, although it has a similar structure to ATF2[31].

ATF7 ubiquitously distributes in fetal or adult mice at a low level and exhibits enhanced expression in specific tissues, including parts of brain and squamous[32]. *Atf7*-deficient mice show abnormal behaviors which partially resemble those of WT mice experienced isolation stress. The ablation of ATF7 increases the expression of 5-HT (serotonin) receptor 5B (*Htr5b*) in the dorsal raphe nuclei of the brain. ATF7 can recruit the histone H3K9 trimethyltransferase ESET to 5’ regulatory region of *Htr5b* and promote the formation of a heterochromatin-like structure to repress its

expression. Social isolation stress stimulates p38-mediated phosphorylation of ATF7 and therefore the release of ATF7 and ESET from the promoter of the serotonin receptor 5b gene (Htr5b), leading to the up-regulation of *Htr5b*[33]. In macrophages, ATF7 silences a group of innate immunity genes by binding with G9a. Pathogen infection-induced phosphorylation of ATF7 leads to a decrease in repressive histone H3K9me2 levels and elevated gene expression[34](Fig. 1-1, B). In response to TNFα treatment, ATF7 mediates stress-induced telomere shortening via release of telomerase from the telomere and/or the regulation of transcription of telomere repeat containing RNA (TERRA) (unpublished data).

2. Transcriptional control of adipocyte development and function

2.1 Types of adipocytes

The adipose tissues are the critical organs for whole-body energy homeostasis. The primary function of white adipose tissue (WAT) is to store the excess energy in form of lipids in unilocular white adipocytes and release fatty acids when food is limited[35]. In small mammals and human, BAT is organized as a special fat depot which protects against hypothermia via dissipation of energy into heat. Brown adipocytes are characterized by abundant mitochondria and the multilocular lipid droplets structure. The thermogenic capacity of brown adipocytes is enabled by UCP1, which locates in the inner mitochondrial membrane[36]. UCP1 uncouples the oxidative phosphorylation from ATP synthesis by catalyzing the proton leak to convert the chemical energy into heat[37]. Recent studies demonstrate that UCP1-positve thermogenic adipocytes also

exist in the white adipose depots, particularly in the subcutaneous adipose tissue. These brown-like adipocytes, termed beige adipocytes, are highly inducible by cold exposure and other environmental cues[38]. Since activation of BAT can increase whole-body energy expenditure and improve energy balance in human, proteins involved in the development and functions of brown and beige adipocyte are attractive therapeutic targets for combating obesity and obesity-related diseases[39,40].

2.2 Origins of adipocytes

Classic BAT depots develop earlier than WAT during prenatal stages. Brown adipocytes originates from the progenitors in the somites. These mesenchymal precursors are marked by activation of certain transcription factors, including myogenic factor 5 (Myf5), paired box 7(Pax7), and the homeobox gene Engrailed-1 (En1). Interestingly, many muscle-specific genes express in the brown adipocyte precursors, supporting the notion that skeletal muscle cells and brown adipocytes share the same progenitors[41,42]. The cell-fate switch between brown adipocytes and muscle cells is controlled by many transcriptional regulators, including early B cell factor 2 (EBF2), PR-domain-containing protein (PRDM16), zinc finger protein 516 (ZFP516), and TATA-binding protein associated factor 7L (TAF7L)[28,43-44] (Fig. 1-2, A).

Despite many biochemical characteristics shared by beige adipocytes and brown adipocytes, the progenitors of these two types of thermogenic cells are different[45]. However, the origins of beige cells are still under debate. The notion of

trans-differentiation of white adipocytes to multilocular beige adipocytes after cold exposure has been supported by several studies[46,47]. In contrast, a number of studies indicate that beige adipocytes originate from distinct sources[48,49]. Myosin heavy chain 11 (Myh11)-positive smooth muscle-like precursors can give rise to a subset of beige cells in the inguinal(i) WAT [50]. Perivascular platelet-derived growth factor receptor-α (*PDGFRα*)-positive precursors in the epididymal (e) WAT are the potential sources of β3 agonist-induced beige adipocytes and these cells also differentiate to white adipocytes[51]. Recently, the mural cells in the white adipose tissue have been demonstrated to be an important source of cold-induced beige adipocytes. These smooth muscle actin(SMA)-positive precursors are also able to differentiate into white adipocytes in the presence of certain stimuli, indicating that beige and white adipocytes originate from the same precursors[52] (Fig. 1-2, B).

2.3 Transcriptional regulation of adipocyte differentiation

The transcriptional cascade in the regulation of the adipocytes differentiation are highly conserved between white and brown adipocytes, although they are derived from distinct cell lineages[53]. Three CCAAT/enhancer-binding protein family members (C/EBPβ, C/EBPa, and C/EBPδ) and PPARγ are the master transcription factors that control the processes of both brown and white adipocyte differentiation. C/EBPβ and C/EBPδ rapidly express after adipogenic induction. These two early regulators induce C/EBPa and PPARγ expression. C/EBPa and PPARγ can cross-regulate each other in a positive-feedback loop and synergistically

promote cell differentiation into mature adipocytes by activating the adipocyte gene program [54]. The process of adipogenesis is also regulated by many other transcriptional factors, including the interferon regulatory factor (IRF) families[55], GATA2/3[56], STAT5A/B[57], and the members of the Krüppel-like factor (KLF) family[54]. Recently, Zinc Finger E-Box Binding Homeobox 1(ZEB1) was identified as a critical pro-adipogenic transcriptional factor of fat cell differentiation[58].

During brown adipogenesis, the transcriptional activity and expression of the key transcription factor are regulated in a different way compared to that of white adipogenesis. Many cell type-specific regulators contribute to brown and beige adipocytes differentiation. Prdm16 interacts with PPARγ and activates its transcriptional function to stimulates brown adipogenesis [59]. It also can form a transcriptional complex with C/EBPβ to initiates brown adipogenesis from myoblastic precursors[60]. Prdm16 recruits the histone methyltransferase Ehmt1 to silence white fat-selective genes and muscle-selective gene in brown adipocytes to control the cell fate and identity of brown adipocytes[61,62]. In subcutaneous white adipose tissue, prdm16 is also essential for beige cell biogenesis[63]. EBF2 recruits PPARγ to its brown fat-specific binding sites to promote brown adipogenesis and the beige adipocytes biogenesis in white adipose tissue[43,64]. ZFP516 associates with Prdm16 to promote the brown and beige adipogeneis[28] (Fig. 1-2, A and B).

2.4 Transcriptional regulation of adipocyte thermogenesis

The thermogenic genes expression in brown and beige adipocytes can be induced by various external cues, including cold exposure, cancer cachexia, exercise and enriched environment[65]. The development and function of thermogenic adipocytes are regulated by these environmental stimuli via various endocrine factors, including catecholamines, interleukin(IL) 6, IL13, IL4, irisin, meteorin-like (METRNL) and FGF21. These endocrine factors are released from metabolically active organs, such as brain, liver, muscle and heart[35](Fig.1-2, C).

Adipose tissues are innervated by the sympathetic nervous system (SNS) which releases norepinephrine in response to cold to activate the β3-adrenergic receptor[66]. The alternative activation of adipose tissue macrophages induced by cold exposure, release catecholamines to activate the expression of thermogenic genes as well[67](Fig.1-2, C).

The induction of thermogenic genes in response to cold stimulus is largely mediated by activation of β-ARs. Adenylyl cyclase activated by β-ARs increases the concentration of cyclic AMP, leading to the enhanced activity of protein kinase A (PKA). PKA induces the phosphorylation of transcription factor CREB and p38, which stimulates the phosphorylation of transcriptional factor ATF2 and the transcriptional co-activator peroxisome proliferator-activated receptor gamma coactivator 1-alpha (PGC1α). These transcriptional regulators bind to regulatory regions of thermogenic genes to activate the thermogenesis[68]. As a master regulator of mitochondria biogenesis, PGC1α can interact with various transcriptional regulator to control the thermogenic gene program. IRF4 is activated by cold exposure and forms

the complex with PGC1α to bind the *Ucp1* gene regulatory regions, resulting in the activation of UCP1 expression[69]. PGC1α also associates with mediator complex subunit 1(MED1) to stimulate the *Ucp1* transcription[70]. In response to cold and sympathetic stimulation, Zfp516 is induced through the cAMP-CREB/ATF2 pathway and interacts with PRDM16 to promote the transcription of *Ucp1* [28](Fig. 1-2, C).

3. The influences of in vitro fertilization on metabolism

Assisted reproductive technologies (ARTs), including in vitro fertilization (IVF), are increasingly used for infertility treatment in humans. More than 6 million children have been conceived through IVF and other ARTs[71]. Although ARTs are thought to be safe, multiple studies suggest that children and adolescents conceived by IVF are at increased risk of metabolic diseases, due to elevated blood pressure, fasting glucose, and peripheral body fat[72,73]. In particular, young adults conceived by IVF display reduced insulin sensitivity and may be more susceptible to the deleterious metabolic consequence of obesogenic environment[74]. Animal studies further confirm the influence of IVF on metabolism at later developmental stages. IVF alters the composition of lipid in mouse fetal liver, and adult mice conceived by IVF display increased fasting glucose levels and impaired glucose tolerance[74,75]. The metabolome in adult fat and liver is also altered by IVF, and metabolites enriched in steroidogenesis and pyrimidine metabolism are elevated by IVF[76].

Accumulating evidence in the Developmental Origins of Health and Disease (DOHaD) field supports the idea that stressful events in early development stages

increase susceptibility to chronic diseases in later life[77]. The IVF procedure exposes the gametes and embryo to an environment that dramatically deviates from natural conception. Manipulation and culture in vitro of gametes and early embryo during IVF would introduce several external stimuli, such as high oxygen, pH and temperature fluctuations, and mechanical stress, which induce stress-activated responses of gametes and embryo[78,79]. The preimplantation embryo is particularly vulnerable to environment disturbances, and these stressful factors could alter the development trajectory of the embryo, leading to long-term effects on gene expression patterns at later stages[77,80]. IVF induces gene expression pattern changes in blastocysts, placenta, and adult tissues, including skeletal muscle, fat, liver, and islets[81,82].

Epigenetic regulation of gene expression is mainly mediated by DNA methylation, post-translational histone modifications, and non-coding RNA. Substantial research indicates that IVF increases the risk of imprinting diseases, such as Beckwith-Wiedemann syndrome, by affecting epigenetic reprogramming and resulting in alteration of gene expression[83,84]. Children conceived by IVF exhibit altered DNA methylation at imprinted genes, such as *MEST* and *H19/IGF2*[85-86]. Recent study also indicates that IVF can induce the dysregulation of microRNAs in mouse embryo, particularly the down-regulation of miR-199a-5p which is involved in regulation of glucose metabolism[87]. Furthermore, IVF alters histone modification at the promotor region of the gene encoding thioredoxin-interacting protein, which plays an important role in glucose and redox hemostasis, in blastocysts and adult adipose tissues [82]. However, the molecular mechanism underlying the lasting effects of IVF on

alteration of metabolic homeostasis through epigenetic reprogramming remains elusive.

Chapter 1. The role of ATF7 in adipocytes development and function

Although the functions of ATF7 in macrophage and brain have been studied, the metabolic role of ATF7 has not been characterized. Previous studies show that *Drosophila* ortholog dATF2 contributes to the regulation of fat metabolism[9] and the other two members ATF2 and CRE-BPa in the mammalian ATF2 family of transcription factors are required for adipocytes differentiation[23]. Especially, it has been well established that ATF2, as a key transcriptional regulator, controls of energy expenditure via induction of thermogenic gene program in response to environmental cues[68]. Thus, we speculated that ATF7 might also be involved in the regulation of metabolic processes. Here, using *Atf7*$^{-/-}$ mice, the involvement of ATF7 in metabolism was investigated.

1. Methods

1.1 Mice

ATF7-deficient (*Atf7*$^{-/-}$) mice were generated as described previously[33]. The *Atf7*$^{-/-}$ and wild-type (WT) littermates used in this study were derived from *Atf7* heterozygotes on a C57BL/6 background. From 6 weeks old, male mice were fed a standard chow diet (CD) or a HFD (60% of kcal from fat). At 5 months old, body fat percentage was measured by dual-energy X-ray absorptiometry (DEXA) analysis using a Lunar PIXImus densitometer. Experiments were conducted in accordance with the guidelines of the Animal Care and Use Committee of the RIKEN Institute.

1.2 Western blotting

Protein extracts were prepared by homogenization in radioimmunoprecipitation (RIPA) buffer (50 mM Tris, pH 8.0, 150 mM sodium chloride, 0.1% SDS, 0.5% sodium deoxycholate ,1.0% NP-40 and protease inhibitors). Proteins were separated on the SDS-polyacrylamide gel (SDS-PAGE) and transferred to PVDF membrane. After treated with the primary antibody at 4 °C overnight, the blots were incubated with a peroxidaseconjugated secondary antibody (Santa Cruz Biotechnology) followed by ECL detection (GE Healthcare) according to the manufacturer's instruction.

1.3 Quantitative-RT PCR

The total RNA was extracted using TRIzol (Invitrogen) and the RT-PCR was performed on 7500 Fast Real-time PCR System using OneStep SYBR Green PCR mix (Takara) following the manufacturer's instructions. The reference gene *TBP* was used as relative control and data were analyzed using the $2^{-\Delta\Delta Ct}$ method.

1.4 Microarray preparation and data analysis

The inguinal WAT samples were isolated from 5-week-old male mice and total RNA was extracted using TRIzol (Invitrogen). Samples were analyzed by microarray using the mouse Gene 1.0 ST Array (Affymetrix). The data were analyzed using linear models for microarray data (Limma) package. The differentially expressed genes (DEGs) were defined with a P-value of ≤ 0.05 and an absolute Log2 fold-change of ≥ 0.5. The raw CEL files of gene expression profiles in iWAT after cold exposure

were downloaded (GEO number: GSE13432) and re-analyzed. Statistical significance of the overlap was examined by Fisher's exact test.

1.5 Isolation of stromal vascular cells and mature adipocytes

The iWATs were dissected from 6-8 weeks old male mice and then digested in the digestion buffer (10 mM $CaCl_2$, 2% BSA, 1 mg/ml collagenase in PBS) for 90 minutes at 37 ℃, followed by washing with DMEM medium containing 10% FBS. The digested tissues were filtered with 70μM cell strainers and the flow-through was centrifuged at 450 x g for 5 min. The stromal vascular cells were pelleted and the mature adipocytes were separated as the floating layer.

1.6 In vitro adipocytes differentiation

The SVF cells were cultured in DMEM medium (20% FBS) until confluence and then exposed to induction medium (10% FBS, 2.85 μM insulin, 0.3 μM dexamethasone (DEXA) and 0.63 mM 3-Isobutyl-1-methylxanthine (IBMX) in DMEM) for 4 days followed by cultivation in the differentiation medium (10% FBS, 200 nM insulin and 10 nM T3 in DMEM) for 4 days.

C3H10T1/2 cells were treated with BMP-2 (100 ng/ml) at 70% confluence in DMEM containing 10% FBS for 3 days and cultured in induction medium (10% FBS, 10 μg/ml insulin, 0.25 μM DEXA and 0.5 mM IBMX in DMEM) for 2 days, and then cultured in the differentiation medium (10% FBS, 10μg/ml insulin in DMEM) for 6 days.

1.7 Oil red O staining

Differentiated cells were washed with PBS twice and fixed with 10% formalin for 1 h. Then cells were washed with 60% isopropanol followed by staining with the Oil Red O working solution for 30 min. The cells were washed with water for 4 times and pictures were taken. Oil Red O was eluted by 100% isopropanol and the OD value at 490 nm was measured.

1.8 Histology and immunohistochemistry

Adipose tissues were isolated from mice and fixed in 4% paraformaldehyde overnight at 4 °C. Paraffin sections were cut at 5μm thick and deparaffinized, rehydrated, and then stained with hematoxylin and eosin. Immunohistochemistry was performed according to the ABC method using PK-6101 (Vector Laboratories) following the manufacturer's instructions. Briefly, the sections were treated with the rabbit polyclonal anti-UCP1 primary antibody at 200× dilution after antigen retrieval and blocked with the blocking buffer (2% bovine serum albumin and 10% normal serum in PBS). The sections were then incubated with the biotinylated anti-rabbit antibody, followed by incubation with avidin-biotin-horseradish peroxidase complex. The labeling was detected with 2,3’-diaminobenzidine tetrahydrochloride (DAB) and examined with light microscope.

1.9 Lentivirus production

To construct the ATF7-overexpression plasmid, the cDNA of mouse ATF7 was amplified and inserted into the vector plenti6.3/TO/V5-GW/lacZ (Life Technologies).

The vector plenti6.3/TO/V5-GW/Flag-ATF7 or plenti6.3/TO/V5-GW/dsRed was transfected into 293T cells with the packing plasmids. The fresh supernatants were collected and filtered through 4.5 syringe filters.

1.10 Plasma parameters

Serum glucose, triglycerides, and cholesterol concentrations were measured using an automatic clinical biochemistry analyzer (JCA-BM6070, JEOL). Serum insulin and resistin levels were measured using the Bio-plex system (Bio-Rad Laboratories).

1.11 Glucose and insulin tolerance tests

At 14 weeks of age, glucose tolerance testing was performed after fasting for 16 h. Glucose solution (2 g/kg body weight) was injected intraperitoneally into mice. Blood glucose levels were measured before (0 min) and 15, 30, 60, and 120 min after glucose injection, using a Glucocard hand-held analyzer (Arkray, Inc). Insulin tolerance testing was performed after a 4 h fast; mice were injected intraperitoneally with recombinant human insulin (Eli Lilly, 0.75 IU/kg of body mass), and then blood glucose was measured before (0 min) and 30, 60, and 90 min after insulin injection.

1.12 Energy expenditure

Energy expenditure was evaluated using indirect calorimetry, by measuring oxygen consumption. Briefly, 12-week-old mice were placed in calorimetric chambers for 48

h. After acclimation of mice to the chambers for 24 h, the volumes of O_2 consumed and CO_2 produced were recorded for ~21 h.

2. Results

2.1 Atf7$^{-/-}$ mice show lower body mass

Atf7$^{-/-}$ mice appeared leaner than their WT littermates (Fig. 2-1, A); therefore, the body masses of *Atf7*$^{-/-}$ and WT mice fed with a CD and HFD were compared. *Atf7*$^{-/-}$ mice on a CD had a significantly lower body mass compared to WT littermates (Fig. 2-1, B). When challenged with a HFD, *Atf7*$^{-/-}$ mice gained less mass relative to WT littermates (Fig. 2-1, B), suggesting that deficiency in ATF7 ameliorates diet-induced obesity. We measured a variety of metabolic parameters in the blood of 11- and 18-week-old mice. There was no difference in serum cholesterol levels between *Atf7*$^{-/-}$ and WT control mice (Fig.2-1, C), whereas *Atf7*$^{-/-}$ mice displayed reduced serum triglycerides, particularly in 18-week-old mice (~50% lower than WT) (Fig. 2-1, D).

2.2 Effects of ATF7 deficiency on adipose tissue

We examined the body composition of the mice using DEXA. Consistent with the reduced body mass of *Atf7*$^{-/-}$ mice, the percentage body fat of *Atf7*$^{-/-}$ mice was lower than that of WT littermates when fed either a CD or a HFD (Fig. 2-2, A). There was no difference in liver mass relative to total body mass between *Atf7*$^{-/-}$ and WT

littermates (Fig. 2-2, B). However, the masses of adipose tissue depots, including eWAT, iWAT, and BAT, were significantly decreased in *Atf7*$^{-/-}$ mice (Fig. 2-2, B). Histological analysis revealed that *Atf7*$^{-/-}$ mice possessed smaller adipocytes than WT mice (Fig. 2-2, C), suggesting that the reduction in adipose tissue mass may have been caused by impaired adipocyte differentiation. Because adipose tissues are the important endocrine organs, we measured serum adipocytokines levels and found that there was on significant difference in serum leptin and adiponectin between *Atf7*$^{-/-}$ and WT littermates (data not shown). By contrast, serum resistin was reduced by ~50% in *Atf7*$^{-/-}$ mice (Fig. 2-2, D).

2.3 Atf7$^{-/-}$ *mice demonstrate increased insulin sensitivity*

Atf7$^{-/-}$ mice exhibited a tendency for fasting serum insulin levels to be reduced (P = 0.08), although similar levels of fasting blood glucose were observed in WT and *Atf7*$^{-/-}$ mice on both diets (Fig. 2-3, A and B). Blood glucose increased to comparable levels during glucose tolerance testing of WT and *Atf7*$^{-/-}$ mice on a CD (Fig. 2-3, C) and after mice had been fed a HFD for 5 months (Fig. 2-3, D). However, blood glucose was significantly more suppressed during insulin tolerance testing in *Atf7*$^{-/-}$ mice than in WT mice on a CD (Fig. 2-3, E). Since long-term HFD feeding can induce the development of insulin resistance, we also assessed the systemic insulin sensitivity of mice on a HFD. Consistent with the effect of genotype on mice fed a CD, ablation of ATF7 ameliorated HFD-induced resistance, indicated by improved suppression of blood glucose levels during an insulin tolerance test (Fig. 2-3, F).

2.4 Atf7$^{-/-}$ mice on a HFD demonstrate increased energy expenditure

ATF2 mediates adaptive thermogenesis by modulating transcription of thermogenic genes[28]. Furthermore, fat mass and adipocyte size were reduced in *Atf7*$^{-/-}$ mice as described above. Therefore, we postulated that ATF7 might also participate in the regulation of energy metabolism. We measured food intake and found that it was not different between *Atf7*$^{-/-}$ mice and their WT littermates (Fig. 2-4, A). Next, we determined energy expenditure by measuring oxygen consumption at room temperature and found that *Atf7*$^{-/-}$ and WT mice on a CD displayed similar levels of energy expenditure (Fig. 2-4, B and C). However, higher oxygen consumption was observed in *Atf7*$^{-/-}$ mice on a HFD during both phases of the circadian cycle (Fig. 2-4, D and E). This implies that the resistance of *Atf7*$^{-/-}$ mice to diet-induced obesity may be due partially to increased energy expenditure.

2.5 Ablation of ATF7 promotes the thermogenic gene program

To investigate the role of ATF7 in adipose tissues, the protein level of ATF7 in BAT, iWAT and eWAT was examined using western blotting and the results indicated that ATF7 expressed in all of these fat tissues at comparable level (Fig. 2-5, A). However, the UCP1 expression level was higher in the iWAT of *Atf7*$^{-/-}$ mice compared to that of WT control, although the difference in BAT between *Atf7*$^{-/-}$ and WT mice was not detected (Fig. 2-5, B). Histological analysis showed that more multilocular adipocytes enriched in iWAT of *Atf7*$^{-/-}$ mice and immunohistochemical staining using anti-UCP1 antibody demonstrated that these multilocular adipocytes were

UCP1-postive and more abundant UCP1 was detected in the iWAT of *Atf7*$^{-/-}$ mice compared to WT.

To explore the changes of gene expression pattern of iWAT induced by ATF7 ablation, we performed microarray analysis and identified 251 genes were up-regulated in *Atf7*$^{-/-}$ mice. We compared this gene lists with cold exposure-induced up-regulated genes and found there was a significant overlap between these two datasets ($P < 0.001$). The top 20 genes containing 14 genes which were also induced by cold exposure, include several key thermogenic genes, such as Ucp1 and Ppargc1a (Fig. 2-5, C), implying that ATF7 is involved in the cold-induced thermogenic gene program. To further explore the function of ATF7 in cold-induced thermogenesis, the mice were exposed to 4 °C for 1h and then the phosphorylation levels of ATF7 was examined. Cold exposure could increase the phosphorylation level of ATF7(Fig. 2-5, E). The UCP1 expression in BAT was higher elevated in *Atf7*$^{-/-}$ mice compared to WT after 24 h cold exposure (Fig. 2-5, F). These data suggest that ATF7 acts as a transcriptional repressor in the cold-induced thermogenic gene program.

2.6 ATF7 positively regulates the adipogenesis

To examine the function of ATF7 in adipocyte development, we measured the ATF7 mRNA expression in stromal vascular cells and mature adipocytes. There was no significant difference between SVF and mature adipocytes in the level of ATF7 in both of BAT and iWAT (Fig. 2-6, A). Stromal vascular cells were induced to differentiate into adipocytes and Oil Red O staining was performed to measure the

lipid amount. The adipogenesis was impaired by ablation of ATF7 and the expression levels of key transcription factors, including C/EBPα, C/EBPβ, and PPARγ, were reduced in *Atf7*$^{-/-}$ cells (Fig. 2-6, B and C). We also determined the effect of ATF7 overexpression on adipogenesis using C3H10T1/2 cell. The elevated ATF7 could promote adipogenesis as indicated by the results of Oil Red O staining and increase the expression levels of C/EBPα and C/EBPβ (Fig. 2-6, D and E). Therefore, we conclude that ATF7 functions as positive regulator during adipocyte development.

3. Discussion

3.1 The role of ATF7 in diet-induced obesity and insulin resistance

The growing epidemic of obesity poses serious health risks due to the development of obesity-associated diseases including type 2 diabetes, hypertension, heart diseases, and cancer[88]. Overconsumption of calorie-dense foods and a sedentary lifestyle are thought to be the two most important factors responsible for the steep increase in the prevalence of obesity worldwide [89]. Here, we showed that the absence of ATF7 in mice results in resistance to diet-induced obesity and reduced serum triglycerides. Lower level of plasma resistin can reverse HFD-induced hepatic insulin resistance[90]. Serum levels of resistin were 50% lower in *Atf7*$^{-/-}$ mice than in their WT littermates, indicating that ATF7 ablation may also alter the endocrine function of adipose tissue,

which may be associated with the improved systemic insulin sensitivity in *Atf7*$^{-/-}$ mice.

The presence of obesity is closely associated with the development of insulin resistance[91]. Thus, we wondered whether the reduced body weight and fat mass of *Atf7*$^{-/-}$ mice would be associated with improved systemic insulin sensitivity in mice fed either a RD or a HFD. In fact, ATF deficiency did not alter glucose tolerance and there was no difference in serum glucose concentration between *Atf7*$^{-/-}$ and WT mice, although this may be due to the decreased serum insulin observed in *Atf7*$^{-/-}$ mice. Of relevance, ATF2 cooperates with other transcription factors, including MafA, to increase transcription of the insulin gene in β-cells[21]. If, conversely, ATF7 reduces insulin gene expression, *Atf7*$^{-/-}$ mice should exhibit a higher serum insulin. Thus, the molecular mechanism underlying the observed decrease in serum insulin in *Atf7*$^{-/-}$ mice may not be simple.

3.2 The role of ATF7 in adipogenesis

Atf7$^{-/-}$ mice exhibited lower fat mass and smaller adipocytes, suggesting that ATF7 may be involved in the regulation of adipose tissue differentiation. The results of in vitro differentiation using SVF and C3H10T1/2 cell line supports this notion. The deficiency of ATF7 impairs the adipogenesis and overexpression of ATF7 promotes adipocytes development. These data are in line with the observations that ATF7 interacts with several key transcription factors, such as C/EBPβ[92] and ZEB1[58] during

adipogenesis, supporting that ATF7 positively regulates the process of adipocyte differentiation.

ATF2 and ATF7 are thought to bind to the same target DNA sequences. Furthermore, both ATF2 and ATF7 were recently identified as proteins that interact with C/EBPβ and ZEB1[58,92]. ATF2 is required for WAT differentiation[23], while ATF2 and ATF7 have opposite effects on transcription of target genes, activating and silencing transcription, respectively[5]. Based on this, we speculated that loss of ATF7 might enhance the differentiation of adipose tissue, but in fact *Atf7*$^{-/-}$ mice exhibited lower adipose tissue mass. Thus, the molecular mechanisms whereby ATF7 regulates adipocyte differentiation may be more complex than predicted.

3.3 The role of ATF7 in the thermogenic gene induction

The development of obesity is tightly linked to the dysregulation of energy balance[93], whereby an imbalance between food intake and energy expenditure leads to the development of obesity and insulin resistance. There were no differences in food intake and energy expenditure between WT and *Atf7*$^{-/-}$ mice on a RD, indicating that the lean phenotype of the *Atf7*$^{-/-}$ mice is not due to an imbalance between food intake and energy expenditure. However, *Atf7*$^{-/-}$ mice fed a HFD showed higher energy expenditure during both light and dark phases, implying that ATF7 may contribute to the regulation of adaptive thermogenesis.

ATF2 is involved in increasing energy expenditure by both directly and indirectly activating transcription of the UCP1 gene[25,28], implying that ATF7 may also contribute to the regulation of thermogenic gene program. Loss of the ATF7 increases the UCP1 gene expression in iWAT at room temperature and in BAT after cold exposure, suggesting that ATF7 has an opposite function in the regulation of adaptive thermogenesis. ATF7 represses rather than activates the thermogenic gene transcription.

According to previous studies which indicate the ATF7 contributes to stress-induced epigenetic changes[33,34], we speculate that ATF7 may silence the thermogenic genes via recruitment of histone methyltransferase to regulatory regions of genes. The loss of ATF7 changes epigenetic status of the thermogenic genes, leading to the activation of transcription and the formation of beige adipocytes. It has been reported that ATF7 can associate with C/EBPβ, which plays the critical role in brown and beige adipocytes differentiation[60,94], at early stage of adipogenesis[92]. Thus, it is also possible that ATF7 inhibits the transcriptional activity of C/EBPβ during processes of brown and beige adipocytes development. The enhanced transcriptional activity of C/EBPβ would promote the formation of beige adipocytes and function of thermogenic adipocytes in *Atf7*$^{-/-}$ mice.

One reason why increased energy expenditure was observed when *Atf7*$^{-/-}$ mice were fed a HFD, but not a RD, could be the high fat diet-induced thermogenesis at neural temperature. The up-regulated UCP1 was observed when mice or rat fed with

high-fat diet[95,96]. We speculate that increased production of ROS in mice fed a HFD results in p38 activation[97], and thus may induce higher levels of ATF7 phosphorylation and the reduction of inhibitory effect of ATF7 on the thermogenic genes transcription.

Alternatively, loss of ATF7 could contribute to enhanced energy expenditure via altered macrophage activity. Cold exposure can also stimulate muscle and adipose tissue to release factors that recruit macrophages to the iWAT, also resulting in induction of thermogenic genes[98,99]. We previously reported that ATF7 could regulate macrophage function via the p38 signaling pathway[34]; thus ATF7 may regulate energy expenditure by promoting macrophage-dependent browning.

In conclusion, our data demonstrated that ATF7 contributes to the regulation of metabolism in mice. Ablation of ATF7 improves the diet-induced obesity and insulin sensitivity. ATF7 controls the energy balance via regulation of adipocyte development and thermogenic gene transcription, providing a possible therapeutic target for obesity and type 2 diabetes, although the understanding of molecular mechanism needs further research.

Chapter 2. ATF7 mediates *in vitro* fertilization-induced gene expression changes in mouse liver

The long-term effects of in vitro fertilization (IVF) on metabolism have been demonstrated in humans and mice[77]. Accumulating evidences suggest that IVF-induced epigenetic reprograming can be maintained at the later stages, leading to the changes of gene expression[84]. However, the mechanism is still elusive. The previous study indicates that *Drosophila* ATF2 (dATF2), the ATF7 homolog, mediates stress-induced epigenetic changes in germ cells and early embryo[11]. Thus, we speculated that ATF7 might also play a role in stress-induced epigenetic changes in gametes and early embryos during the IVF process, and might contribute to gene expression changes in the specific tissues at later stages.

1. Methods

1.1 Mice and IVF

Atf7$^{-/-}$ mice were generated as described previously[33]. Using *Atf7*$^{+/-}$ heterozygote mature female and male mice (C57BL/6 background), wild-type (WT) and *Atf7*$^{-/-}$ progeny were produced by IVF or natural mating. IVF was performed as follows. Sperm were collected from the caudae epididymides of male mice, and allowed to diffuse in fertilization medium. After preincubation for approximately 1 h to allow for capacitation, the sperm were used for insemination. Meanwhile, female mice were superovulated using intraperitoneal injections of pregnant mare's serum gonadotropin and human chorionic gonadotropin (hCG) (Serotropin and Gonatropin; ASKA

Pharmaceutical Co.) with an interval of 48 h between injections. Approximately 15–17 h after the hCG injection, the oocytes-cumulus complexes were collected from the oviducts of superovulated female mice. The complexes from several female mice were placed in fertilization medium. Insemination was performed by adding the preincubated sperm suspension to the fertilization medium containing complexes and culturing at 37 °C with 5% CO_2 in air. Twenty-four hours after insemination, 2-cell embryos were transferred into the oviducts of pseudopregnant ICR females (CLEA Japan, Tokyo, Japan) mated to vasectomized ICR males.

1.2 Gene Expression Analysis Using Array

The liver samples were isolated from 4-week-old male mice derived from natural mating or IVF. Total RNA was extracted using TRIzol (Invitrogen) based on the manufacturer's protocol. Single-strand cDNA was prepared with WT Expression Kit (Ambion) and then labeled using the WT terminal labeling kit (Ambion) according the manufacturer's manual. Samples were analyzed by microarray using the Mouse Gene 1.0 ST Array (Affymetrix). The raw (CEL) data were normalized using the RMA method in the R package *affy*, and the comparisons of gene expression were implemented using the linear models for microarray data (Limma) package[100]. The differentially expressed genes (DEGs) were defined with an adjusted P-value of ≤ 0.05 and an absolute $\log_2$ fold-change ($\log_2$FC) of ≥ 0.6. The pathways enrichment analysis for DEGs was conducted using the Kyoto Encyclopedia of Genes and Genomes (KEGG) database[101]. Hierarchical clustering analysis was performed using the *log_2 signal intensity* of IVF-induced DEGs in WT mice.

1.3 Quantitative RT-PCR

RT-PCR was performed using OneStep SYBR Green PCR mix (Takara) following the manufacturer's instructions. The qRT-PCR was performed using a 7500 Fast Real-time PCR System (Applied Biosystems). Primers GGCTCCTCTATGATGGCCG and AAGCCTTTCTGAACAGCCAGC were used for *Mest*; primers AACGGTGGAGATGGATTCCAGATG and GACTTGCTGCAGAGAACTTGATCC were used for *Nt5e*; primers TCAGTGTACCATGATTGCCTTG and GAACCTGCTCTGCCTGTTG were used for *Idi1*; primers GCTCCAAGCAGATGCAGCA and CCGGATGTGAGGCAGCAG were used for *36B4*; and primers GGGTGTCCTCCCTGGAAAAG and TCAGCTGAGCCACCTCATTG were used for *Atf7*. The reference gene *36B4* was used as a relative control, and data were analyzed using the $2^{-\Delta\Delta Ct}$ method.

1.4 Western Blotting

Protein extracts were prepared from liver samples by homogenization in radioimmunoprecipitation buffer (50 mM Tris pH 8.0, 150 mM sodium chloride, 0.1% SDS, 0.5% sodium deoxycholate, 1.0% NP-40, and protease inhibitors). Proteins were separated on a 7.5% SDS-polyacrylamide gel (SDS-PAGE) and then transferred to PVDF membrane. After treatment with the anti-ATF7 monoclonal (1A7) antibody or anti-α-tubulin antibody (Abcam, ab4074) at 4 °C overnight, the blots were incubated with a peroxidase-conjugated anti-mouse IgG1 (Santa Cruz Biotechnology) or anti-rabbit (Invitrogen) secondary antibody followed by ECL detection (GE Healthcare) according to the manufacturer's instructions.

2. Results

2.1 Effect of IVF on gene expression profiles in liver

To explore the gene expression pattern changes induced by IVF, we investigated the liver transcriptome in 4-week-old male mice generated by either IVF or normal mating (control), using an array covering the mouse whole genome transcript with 750,000 unique oligonucleotide probes. This analysis identified 668 genes up- and 204 genes down-regulated in IVF liver compared with the control (Fig. 3-1, A). To investigate the pathways associated with DEGs, the gene lists of up- and down-regulated genes were analyzed for KEGG pathway enrichment using the DAVID database. Thirteen pathways were over-represented among the up-regulated genes, including complement and coagulation cascades, gap junction, and ECM-receptor interaction. Several metabolism-associated pathways were identified, such as pyrimidine metabolism, purine metabolism, and steroid hormone biosynthesis (Fig. 3-1, B). These results are consistent with the report that metabolites enriched in pyrimidine metabolism and steroidogenesis are elevated by IVF[76]. The down-regulated genes were also enriched for genes in metabolic-related pathways, including PPAR signaling, valine, leucine, and isoleucine degradation, and biosynthesis of unsaturated fatty acids (Fig. 3-1, C), implying that IVF mainly disturbs metabolic processes in liver. The circadian rhythm pathway was over-represented among both up- and down-regulated genes. The imprinted gene *Mest* was expressed more highly in IVF liver than in control liver ($\log_2$FC = 0.92, adjusted P-value = 0.03). To verify the microarray data, we examined the relative expression

level of *Mest* by qRT-PCR using *36B4* as an internal control. The result was consistent with the microarray data and indicated that the expression levels of *Mest* were significantly higher in livers of mice conceived by IVF than in livers of control mice (Fig. 3-1, D). As reported previously[80,85,86], the expression level of another imprinted gene *Igf2* was up-regulated by IVF (log2FC = 0.588, adjusted P-value = 0.031), whereas the expression level of *H19* was not affected.

2.2 The influence of IVF on gene expression is reduced in Atf7$^{-/-}$ mice

To explore whether ATF7 is involved in IVF-induced gene expression changes, we first tested the effect of IVF on ATF7 expression levels in liver. There was no difference in *Atf7* mRNA levels between IVF and control livers (Fig. 3-2, A). Using liver from *Atf7*$^{-/-}$ mice as a negative control, western blotting also showed that the level of ATF7 protein in IVF livers is comparable to that in control livers (Fig. 3-2B). Therefore. IVF did not affect the expression of ATF7 in liver.

Next, we explored whether the absence of ATF7 affected the influence of IVF by comparing the liver gene expression profiles between IVF-conceived *Atf7*$^{-/-}$ mice and naturally conceived *Atf7*$^{-/-}$ mice (*Atf7*$^{-/-}$ control). In *Atf7*$^{-/-}$ liver, 508 genes were up- and 825 genes were down-regulated by IVF (Fig. 3-2, C). Comparison of the IVF-induced genes in WT (668 genes) with those in *Atf7*$^{-/-}$ (508 genes) liver indicated that the expression of 87% (596/668 genes) of the IVF-induced genes in WT was not affected by IVF in *Atf7*$^{-/-}$ mice (Fig. 3-2, D). Only 13% (92/668 genes, $P < 0.001$) were induced by IVF in both WT and *Atf7*$^{-/-}$ mice, and these included genes

associated with the circadian rhythm (i.e., *NPAS2*, *ARNTL*, and *CRY1*) and complement and coagulation cascades (i.e., *MBL1*, *F13B*, and *FGA*). The KEGG pathway analysis showed that the IVF-induced genes in *Atf7*$^{-/-}$ liver were enriched for genes in 13 pathways (Fig. 3-2E). Among them, only five pathways were common with those identified for up-regulated genes in WT mice: circadian rhythm, spliceosome, complement and coagulation cascades, proteasome, and steroid hormone biosynthesis. Other pathways identified in WT mice, including purine metabolism and terpenoid backbone biosynthesis, were not observed in *Atf7*$^{-/-}$ mice. These results indicate that a loss of ATF7 abrogated the IVF-induced expression of most of the metabolism-related genes in liver.

2.3 ATF7 ablation can partially mimic the effect of IVF

ATF7 acts as a transcriptional repressor, and mediates stress-induced gene expression. Therefore, *Atf7*$^{-/-}$ mice exhibit some similar phenotypes to WT mice exposed to stress[33,34]. Thus, we compared the gene expression profiles of *Atf7*$^{-/-}$ and WT livers. In *Atf7*$^{-/-}$ liver, 903 genes were up-regulated and 416 genes were down-regulated compared with WT liver (Fig. 3-3, A). Comparison of the 903 up-regulated genes with the 688 IVF-induced genes showed that 37% (255/688 genes) of the IVF-induced genes also exhibited higher expression levels in *Atf7*$^{-/-}$ than in WT mice (Fig. 3-3, B). The 903 up-regulated genes were enriched for genes in 17 pathways (Fig. 3-3, C). The majority of these pathways were closely related to metabolism, including purine and pyrimidine metabolism, steroid biosynthesis, and steroid

hormone biosynthesis, implying that ATF7 plays an important role in regulation of metabolism in liver. Interestingly, six pathways enriched for the IVF-induced genes were common to those enriched for the ATF7 ablation-induced genes, including purine metabolism, pyrimidine metabolism, and terpenoid backbone biosynthesis (Fig. 3-3, C). Hierarchical clustering analysis allows us to visualize the relationship between the different experiment components. By using DEGs identified in IVF versus control, all 12 samples divided into two major clusters. The three WT control samples formed a cluster, and *Atf7*$^{-/-}$ samples from naturally conceived mice grouped together with IVF samples (Fig. 3-3, D). These data further demonstrate the potential role of ATF7 in mediating the IVF-induced gene expression changes, particularly for genes associated with metabolic pathways.

2.4 Gene expression changes in metabolic pathways

Dozens of genes induced by IVF and involved in metabolic pathways were also up-regulated in the *Atf7*$^{-/-}$ control, whereas their expression levels were not increased by IVF in *Atf7*$^{-/-}$ mice. This observation led us to postulate that ATF7 may mainly contribute to IVF-induced up-regulation of genes in metabolic pathways. Hence, we checked the expression profiles of metabolic genes involved in two pathways: purine metabolism and terpenoid backbone biosynthesis. The heat map of expression profiles of genes involved in purine metabolism showed that the majority of genes exhibited higher expression levels in *Atf7*$^{-/-}$ control, *Atf7*$^{-/-}$ IVF, and WT IVF groups than in the WT control (Fig. 3-4, A). This tendency was confirmed by measurement of *Nt5e* mRNA levels using qRT-PCR. *Nt5e* mRNA levels were 10-fold higher in *Atf7*$^{-/-}$

control, *Atf7*$^{-/-}$ IVF, and WT IVF groups than in the WT control (Fig. 3-4, B). However, genes involved in terpenoid backbone biosynthesis were only up-regulated in *Atf7*$^{-/-}$ control and WT IVF groups. Gene expression levels in *Atf7*$^{-/-}$ IVF were not higher than in the WT control (Fig. 3-4, C). Results of qRT-PCR showed that the *Idi1* mRNA level was up-regulated by IVF and ATF7 ablation, but decreased in *Atf7*$^{-/-}$ IVF (Fig. 3-4, D). Expression levels of the transcriptional activator *Srebf2*, which is a key player in lipid metabolism, were higher in the *Atf7*$^{-/-}$ control than in the WT control ($\log_2$FC = 0.754762, adjusted P-value = 0.0004). In the absence of ATF7, IVF led to a reduction in *Srebf2* expression level ($\log_2$FC = -0.68, adjusted P-value = 0.0009). The expression level of *Srebf2* may explain the expression patterns of genes involved in terpenoid backbone biosynthesis and indicates that ATF7 contributes to IVF-induced gene expression changes synergistically with other factors.

3. Discussion

The present study indicates that ATF7 is involved in the memory of IVF-induced gene expression pattern changes in the liver. Our previous study showed that ATF7 silences target genes by forming a heterochromatin-like structure via recruitment of histone H3K9 trimethyltransferase ESET/SETDB1[33] or histone H3K9 dimethyltransferase G9a[34], and that certain stress induces ATF7 phosphorylation by p38, leading to ATF7 release. This causes a decrease in H3K9me3 or H3K9me2 and subsequent transcriptional induction. Once the heterochromatin-like structure is disrupted by stress, it is not completely recovered and the partially disrupted structure

and the higher basal expression level are retained for a long period. A similar scenario may occur in the memory of IVF-induced gene expression changes (Fig. 3-4E). During IVF, especially in vitro culture of zygotes and 2-cell embryos, the level of reactive oxygen species (ROS) is elevated[102] A high level of intracellular glutathione, which reduces ROS, is important for bovine embryo development after in vitro maturation[103]. Since ROS induces p38 activation[104], an increased ROS level during in vitro culture of zygotes and 2-cell embryos leads to ATF7 phosphorylation. According to the Database of Transcriptome in Mouse Early Embryos (http://dbtmee.hgc.jp/gene_card.php?id=2002900), ATF7 is expressed in oocytes, zygotes, and 2-cell embryos at least at low levels. ATF7 phosphorylation and its release from target genes leads to a decrease in H3K9me3 and/or H3K9me2, which is not completely recovered. Thus, a partly disrupted heterochromatin-like structure and high basal expression of some ATF7 target genes may be maintained during development of liver at least until 4 weeks of age.

Metabolism-related genes are over-represented among the IVF-induced genes in 4-week-old liver. These consist of two types of genes, whose expression is directly or indirectly regulated by ATF7. Why does IVF induce the memory of up-regulation of metabolism-related genes? This could be an adaptation to the IVF stress. When zygotes and early embryos are cultured in vitro, cells must adapt to the non-physiological extracellular stimulus via modulation of metabolism, such as the concentration of some metabolites. For example, to combat the higher ROS level during in vitro culture, more antioxidants may be produced. The genes involved in

complement and coagulation cascades are also up-regulated by IVF. Complement is a key system for homeostasis[105], and so those genes may play a role in maintaining homeostasis after receiving IVF stress. These changes may benefit cells when they are exposed to IVF stress, but may induce long-term harmful consequences at later stages after transfer to female recipient mice.

In WT liver, loss of ATF7 canceled the memory of IVF-induced up-regulation of 89% (596/668 genes) of genes. On the other hand, in *Atf7*$^{-/-}$ liver, IVF induced the up-regulation of 416 genes that were not induced in WT liver. This suggests the presence of some back-up system, which acts to induce the memory of the IVF effect in the absence of ATF7. ATF7 is not the only inducer of epigenetic change in response to stress. Two substrates of the Krebs cycle, fumarate and succinate, are competitive inhibitors of multiple α-ketoglutarate-dependent dioxygenases, including histone demethylases and the TET family of 5-methylcytosine hydroxylases involved in DNA demethylation[106]. Therefore, a change in metabolism induced by IVF may cause epigenetic change via those metabolites in the absence of ATF7, although it remains unknown how inhibition of histone demethylases and DNA demethylation affects the epigenetic status of specific genes.

In *Atf7*$^{-/-}$ liver, IVF did not induce the memory of up-regulation of genes involved in purine metabolism, whose expression levels were higher than in WT liver. This suggests that ATF7 suppresses transcription of those genes by forming a heterochromatin-like structure, and that loss of ATF7 or IVF-induced release of ATF7 up-regulated their expression. On the other hand, although the expression of genes in

terpenoid backbone biosynthesis was also up-regulated by a loss of ATF7, IVF oppositely suppressed their expression in *Atf7*$^{-/-}$ liver. This might be caused by inducing some transcriptional repressor by IVF in *Atf7*$^{-/-}$ liver. As described above, some metabolites such as substrates of the Krebs cycle change the epigenetic states of some genes. Such regulation may induce a specific repressor for the genes involved in terpenoid backbone biosynthesis, but not for the genes involved in purine metabolism. It might be interesting to think about the relationship between specific metabolism pathways and adaptation to IVF stress.

This study indicates that ATF7 is a major regulator in inducing the memory of IVF effects. At present, it is difficult to identify ATF7-binding genes in zygotes and 2-cell embryos due to technical limitations. However, in the future, identification of those ATF7 target genes and measurement of the IVF-induced epigenetic changes at those genes will be useful to predict the effect of IVF in adulthood.

References

1. Maekawa T, Sakura H, Kanei-Ishii C, Sudo T, Yoshimura T, Fujisawa J, Yoshida M, Ishii S. Leucine zipper structure of the protein CRE-BP1 binding to the cyclic AMP response element in brain. The EMBO Journal, 1989, 8(7): 2023-2028.

2. Hai TW, Liu F, Coukos WJ, Green MR. Transcription factor ATF cDNA clones: an extensive family of leucine zipper proteins able to selectively form DNA-binding heterodimers. Genes & Development, 1989, 3(12b): 2083-2090.

3. Nomura N, Zu YL, Maekawa T, Tabata S, Akiyama T, Ishii S. Isolation and characterization of a novel member of the gene family encoding the cAMP response element-binding protein CRE-BP1. Journal of Biological Chemistry, 1993, 268(6): 4259-4266.

4. Gaire M, Chatton B, Kedinger C. Isolation and characterization of two novel, closely related ATF cDNA clones from HeLa cells. Nucleic Acids Research, 1990, 18(12): 3467-3473.

5. Seong KH, Maekawa T, Ishii S. Inheritance and memory of stress-induced epigenome change: roles played by the ATF-2 family of transcription factors. Genes to Cells, 2012, 17(4): 249-263.

6. Bhoumik A, Lopez-Bergami P, Ronai Z. ATF2 on the double–activating transcription factor and DNA damage response protein. Pigment Cell Research, 2007, 20(6): 498-506.

7. Jia S, Noma K, Grewal SI. RNAi-independent heterochromatin nucleation by the stress-activated ATF/CREB family proteins. Science, 2004, 304(5679): 1971-1976.

8. Shivers RP, Pagano DJ, Kooistra T, Richardson CE, Reddy KC, Whitney JK, Kamanzi O, Matsumoto K, Hisamoto N, Kim DH. Phosphorylation of the

conserved transcription factor ATF-7 by PMK-1 p38 MAPK regulates innate immunity in Caenorhabditis elegans. PLoS Genetics, 2010, 6(4): e1000892.

9. Okamura T, Shimizu H, Nagao T, Ueda R, Ishii S. ATF-2 regulates fat metabolism in Drosophila. Molecular Biology of the Cell, 2007, 18(4): 1519-1529.

10. Shimizu H, Shimoda M, Yamaguchi T, Seong KH, Okamura T, Ishii S. Drosophila ATF-2 regulates sleep and locomotor activity in pacemaker neurons. Molecular and Cellular Biology, 2008, 28(20): 6278-6289.

11. Seong KH, Li D, Shimizu H, Nakamura R, Ishii S. Inheritance of stress-induced, ATF-2-dependent epigenetic change. Cell, 2011, 145(7): 1049-1061.

12. Lau E, Ze'ev AR. ATF2–at the crossroad of nuclear and cytosolic functions. Journal of Cell Science, 2012, 125(12): 2815-2824.

13. Bhoumik A, Takahashi S, Breitweiser W, Shiloh Y, Jones N, Ronai Z. ATM-dependent phosphorylation of ATF2 is required for the DNA damage response. Molecular Cell, 2005, 18(5): 577-587.

14. Takeda J, Maekawa T, Sudo T, Seino Y, Imura H, Saito N, Tanaka C, Ishii S. Expression of the CRE-BP1 transcriptional regulator binding to the cyclic AMP response element in central nervous system, regenerating liver, and human tumors. Oncogene, 1991, 6(6): 1009-1014.

15. Ackermann J, Ashton G, Lyons S, James D, Hornung JP, Jones N, Breitwieser W. Loss of ATF2 function leads to cranial motoneuron degeneration during embryonic mouse development. PloS One, 2011, 6(4): e19090.

16. Maekawa T, Bernier F, Sato M, Nomura S, Singh M, Inoue Y, Tokunaga T, Imai H, Yokoyama M, Reimold A, Glimcher LH, Ishii S. Mouse ATF-2 null mutants display features of a severe type of meconium aspiration syndrome. Journal of Biological Chemistry, 1999, 274(25): 17813-17819.

17. Lopez-Bergami P, Lau E, Ronai Z. Emerging roles of ATF2 and the dynamic AP1 network in cancer. Nature Reviews Cancer, 2010, 10(1): 65-76.

18. Huguier S, Baguet J, Perez S, van Dam H, Castellazzi M. Transcription factor ATF2 cooperates with v-Jun to promote growth factor-independent proliferation in vitro and tumor formation in vivo. Molecular and Cellular Biology, 1998, 18(12): 7020-7029.

19. Maekawa T, Shinagawa T, Sano Y, Sakuma T, Nomura S, Nagasaki K, Miki Y, Saito-Ohara F, Inazawa J, Kohno T, Yokota J, Ishii S. Reduced levels of ATF-2 predispose mice to mammary tumors. Molecular and Cellular Biology, 2007, 27(5): 1730-1744.

20. Lau E, Kluger H, Varsano T, Lee K, Scheffler I, Rimm DL, Ideker T, Ronai ZA. PKCε promotes oncogenic functions of ATF2 in the nucleus while blocking its apoptotic function at mitochondria. Cell, 2012, 148(3): 543-555.

21. Han S, Yasuda K, Kataoka K. ATF2 interacts with β-cell-enriched transcription factors, MafA, Pdx1, and Beta2, and activates insulin gene transcription. Journal of Biological Chemistry, 2011, 286(12): 10449-10456.

22. Hay CW, Ferguson L A, Docherty K. ATF-2 stimulates the human insulin promoter through the conserved CRE2 sequence. Biochimica et Biophysica Acta (BBA)-Gene Structure and Expression, 2007, 1769(2): 79-91.

23. Maekawa T, Jin W, Ishii S. The role of ATF-2 family transcription factors in adipocyte differentiation: antiobesity effects of p38 inhibitors. Molecular and Cellular Biology, 2010, 30(3): 613-625.

24. Rosen ED, Walkey CJ, Puigserver P, Spiegelman BM. Transcriptional regulation of adipogenesis. Genes & Development, 2000, 14(11): 1293-1307.

25. Bordicchia M, Liu D, Amri EZ, Ailhaud G, Dessì-Fulgheri P, Zhang C, Takahashi N, Sarzani R, Collins S. Cardiac natriuretic peptides act via p38 MAPK to induce the brown fat thermogenic program in mouse and human adipocytes. The Journal of Clinical Investigation, 2012, 122(3): 1022-1036.

26. Enerbäck S, Jacobsson A, Simpson EM, Guerra C, Yamashita H, Harper ME, Kozak LP. Mice lacking mitochondrial uncoupling protein are cold-sensitive but not obese. Nature, 1997, 387(6628): 90 - 94.

27. Cao W, Daniel KW, Robidoux J, Puigserver P, Medvedev AV, Bai X, Floering LM, Spiegelman BM, Collins S. p38 mitogen-activated protein kinase is the central regulator of cyclic AMP-dependent transcription of the brown fat uncoupling protein 1 gene. Molecular and Cellular Biology, 2004, 24(7): 3057-3067.

28. Dempersmier J, Sambeat A, Gulyaeva O, Paul SM, Hudak CS, Raposo HF, Kwan HY, Kang C, Wong RH, Sul HS. Cold-inducible Zfp516 activates UCP1 transcription to promote browning of white fat and development of brown fat. Molecular Cell, 2015, 57(2): 235-246.

29. Diring J, Camuzeaux B, Donzeau M, Vigneron M, Rosa-Calatrava M, Kedinger C, Chatton B. A cytoplasmic negative regulator isoform of ATF7 impairs ATF7 and ATF2 phosphorylation and transcriptional activity. PLoS One, 2011, 6(8): e23351.

30. Sano Y, Tokitou F, Dai P, Maekawa T, Yamamoto T, Ishii S. CBP alleviates the intramolecular inhibition of ATF-2 function. Journal of Biological Chemistry, 1998, 273(44): 29098-29105.

31. De Graeve F, Bahr A, Chatton B, Kedinger C. A murine ATFa-associated factor with transcriptional repressing activity. Oncogene, 2000, 19(14): 1807- 1819.

32. Goetz J, Chatton B, Mattei MG, Kedinger C. Structure and expression of the ATFa gene. Journal of Biological Chemistry, 1996, 271(47): 29589-29598.

33. Maekawa T, Kim S, Nakai D, Makino C, Takagi T, Ogura H, Yamada K, Chatton B, Ishii S. Social isolation stress induces ATF‐7 phosphorylation and impairs silencing of the 5‐HT 5B receptor gene. The EMBO Journal, 2010, 29(1): 196-208.

34. Yoshida K, Maekawa T, Zhu Y, Renard-Guillet C, Chatton B, Inoue K, Uchiyama T, Ishibashi K, Yamada T, Ohno N, Shirahige K, Okada-Hatakeyama M, Ishii S. The transcription factor ATF7 mediates lipopolysaccharide-induced epigenetic changes in macrophages involved in innate immunological memory. Nature Immunology, 2015, 16(10): 1034-1043.

35. Bartelt A, Heeren J. Adipose tissue browning and metabolic health. Nature Reviews Endocrinology, 2014, 10(1): 24-36.

36. Kajimura S, Saito M. A new era in brown adipose tissue biology: molecular control of brown fat development and energy homeostasis. Annual Review of Physiology, 2014, 76: 225-249.

37. Kajimura S, Spiegelman BM, Seale P. Brown and beige fat: physiological roles beyond heat generation. Cell Metabolism, 2015, 22(4): 546-559.

38. Wu J, Cohen P, Spiegelman BM. Adaptive thermogenesis in adipocytes: Is beige the new brown?. Genes & Development, 2013, 27(3): 234-250.

39. Yoneshiro T, Aita S, Matsushita M, Kameya T, Nakada K, Kawai Y, Saito M. Brown adipose tissue, whole-body energy expenditure, and thermogenesis in healthy adult men. Obesity, 2011, 19(1): 13-16.

40. Ohno H, Shinoda K, Spiegelman BM, Kajimura S. PPARγ agonists induce a white-to-brown fat conversion through stabilization of PRDM16 protein. Cell Metabolism, 2012, 15(3): 395-404.

41. Walden TB, Timmons JA, Keller P, Nedergaard J, Cannon B. Distinct expression of muscle‐specific MicroRNAs (myomirs) in brown adipocytes. Journal of Cellular Physiology, 2009, 218(2): 444-449.

42. Timmons JA, Wennmalm K, Larsson O, Walden TB, Lassmann T, Petrovic N, Hamilton DL, Gimeno RE, Wahlestedt C, Baar K, Nedergaard J, Cannon B. Myogenic gene expression signature establishes that brown and white adipocytes originate from distinct cell lineages. Proceedings of the National Academy of Sciences, 2007, 104(11): 4401-4406.

43. Rajakumari S, Wu J, Ishibashi J, Lim HW, Giang AH, Won KJ, Reed RR, Seale P. EBF2 determines and maintains brown adipocyte identity. Cell Metabolism, 2013, 17(4): 562-574.

44. Zhou H, Wan B, Grubisic I, Kaplan T, Tjian R. TAF7L modulates brown adipose tissue formation. Elife, 2014, 3: E02811.

45. Inagaki T, Sakai J, Kajimura S. Transcriptional and epigenetic control of brown and beige adipose cell fate and function. Nature Reviews Molecular Cell Biology, 2016, 17(8): 480-495.

46. Lee YH, Petkova AP, Konkar AA, Granneman JG. Cellular origins of cold-induced brown adipocytes in adult mice. The FASEB Journal, 2015, 29(1): 286-299.

47. Shao M, Ishibashi J, Kusminski CM, Wang QA, Hepler C, Vishvanath L, MacPherson KA, Spurgin SB, Sun K, Holland WL, Seale P, Gupta RK. Zfp423

maintains white adipocyte identity through suppression of the beige cell thermogenic gene program. Cell Metabolism, 2016, 23(6): 1167-1184.

48. Wang QA, Tao C, Gupta RK, Scherer PE. Tracking adipogenesis during white adipose tissue development, expansion and regeneration. Nature Medicine, 2013, 19(10): 1338-1344.

49. Sanchez-Gurmaches J, Hung CM, Sparks CA, Tang Y, Li H, Guertin DA. PTEN loss in the Myf5 lineage redistributes body fat and reveals subsets of white adipocytes that arise from Myf5 precursors. Cell Metabolism, 2012, 16(3): 348-362.

50. Long JZ, Svensson KJ, Tsai L, Zeng X, Roh HC, Kong X, Rao RR, Lou J, Lokurkar I, Baur W, Castellot JJ Jr, Rosen ED, Spiegelman BM. A smooth muscle-like origin for beige adipocytes. Cell Metabolism, 2014, 19(5): 810-820.

51. Lee YH, Petkova AP, Mottillo EP, Granneman JG. In vivo identification of bipotential adipocyte progenitors recruited by β3-adrenoceptor activation and high-fat feeding. Cell Metabolism, 2012, 15(4): 480-491.

52. Berry DC, Jiang Y, Graff JM. Mouse strains to study cold-inducible beige progenitors and beige adipocyte formation and function. Nature Communications, 2016, 7: 10184.

53. Peirce V, Carobbio S, Vidal-Puig A. The different shades of fat. Nature, 2014, 510(7503): 76-83.

54. Siersbæk R, Nielsen R, Mandrup S. Transcriptional networks and chromatin remodeling controlling adipogenesis. Trends in Endocrinology & Metabolism, 2012, 23(2): 56-64.

55. Eguchi J, Yan QW, Schones DE, Kamal M, Hsu CH, Zhang MQ, Crawford GE, Rosen ED. Interferon regulatory factors are transcriptional regulators of adipogenesis. Cell Metabolism, 2008, 7(1): 86-94.

56. Tong Q, Dalgin G, Xu H, Ting CN, Leiden JM, Hotamisligil GS. Function of GATA transcription factors in preadipocyte-adipocyte transition. Science, 2000, 290(5489): 134-138.

57. Floyd ZE, Stephens JM. STAT5A promotes adipogenesis in nonprecursor cells and associates with the glucocorticoid receptor during adipocyte differentiation. Diabetes, 2003, 52(2): 308-314.

58. Gubelmann C, Schwalie PC, Raghav SK, Röder E, Delessa T, Kiehlmann E, Waszak SM, Corsinotti A, Udin G, Holcombe W, Rudofsky G, Trono D, Wolfrum C, Deplancke B. Identification of the transcription factor ZEB1 as a central component of the adipogenic gene regulatory network. Elife, 2014, 3: e03346.

59. Seale P, Bjork B, Yang W, Kajimura S, Chin S, Kuang S, Scimè A, Devarakonda S, Conroe HM, Erdjument-Bromage H, Tempst P, Rudnicki MA, Beier DR, Spiegelman BM. PRDM16 controls a brown fat/skeletal muscle switch. Nature, 2008, 454(7207): 961-967.

60. Kajimura S, Seale P, Kubota K, Lunsford E, Frangioni JV, Gygi SP, Spiegelman BM. Initiation of myoblast to brown fat switch by a PRDM16–C/EBP-β transcriptional complex. Nature, 2009, 460(7259): 1154-1158.

61. Harms MJ, Ishibashi J, Wang W, Lim HW, Goyama S, Sato T, Kurokawa M, Won KJ, Seale P. Prdm16 is required for the maintenance of brown adipocyte identity and function in adult mice. Cell Metabolism, 2014, 19(4): 593-604.

62. Ohno H, Shinoda K, Ohyama K, Sharp LZ, Kajimura S. EHMT1 controls brown adipose cell fate and thermogenesis through the PRDM16 complex. Nature, 2013, 504(7478): 163-167.

63. Seale P, Conroe HM, Estall J, Kajimura S, Frontini A, Ishibashi J, Cohen P, Cinti S, Spiegelman BM. Prdm16 determines the thermogenic program of subcutaneous white adipose tissue in mice. The Journal of Clinical Investigation, 2011, 121(1): 96-105.

64. Stine RR, Shapira SN, Lim HW, Ishibashi J, Harms M, Won KJ, Seale P. EBF2 promotes the recruitment of beige adipocytes in white adipose tissue. Molecular Metabolism, 2016, 5(1): 57-65.

65. Sidossis L, Kajimura S. Brown and beige fat in humans: thermogenic adipocytes that control energy and glucose homeostasis. The Journal of Clinical Investigation, 2015, 125(2): 478-486.

66. Golozoubova V, Hohtola E, Matthias A, Jacobsson A, Cannon B, Nedergaard J. Only UCP1 can mediate adaptive nonshivering thermogenesis in the cold. The FASEB Journal, 2001, 15(11): 2048-2050.

67. Nguyen KD, Qiu Y, Cui X, Goh YP, Mwangi J, David T, Mukundan L, Brombacher F, Locksley RM, Chawla A. Alternatively activated macrophages produce catecholamines to sustain adaptive thermogenesis. Nature, 2011, 480(7375): 104-108.

68. Harms M, Seale P. Brown and beige fat: development, function and therapeutic potential. Nature Medicine, 2013, 19(10): 1252-1263.

69. Kong X, Banks A, Liu T, Kazak L, Rao RR, Cohen P, Wang X, Yu S, Lo JC, Tseng YH, Cypess AM, Xue R, Kleiner S, Kang S, Spiegelman BM, Rosen ED.

IRF4 is a key thermogenic transcriptional partner of PGC-1α. Cell, 2014, 158(1): 69-83.

70. Chen W, Yang Q, Roeder RG. Dynamic interactions and cooperative functions of PGC-1α and MED1 in TRα-mediated activation of the brown-fat-specific UCP-1 gene. Molecular Cell, 2009, 35(6): 755-768.

71. Dyer S, Chambers GM, de Mouzon J, Nygren KG, Zegers-Hochschild F, Mansour R, Ishihara O, Banker M, Adamson GD. International committee for monitoring assisted reproductive technologies world report: assisted reproductive technology 2008, 2009 and 2010. Human Reproduction, 2016, 1(7):1588-609.

72. Ceelen M, van Weissenbruch MM, Roos JC, Vermeiden JP, van Leeuwen FE, Delemarre-van de Waal HA. Body composition in children and adolescents born after in vitro fertilization or spontaneous conception. The Journal of Clinical Endocrinology & Metabolism, 2007, 92(9): 3417-3423.

73 . Ceelen M, van Weissenbruch MM, Vermeiden JP, van Leeuwen FE, Delemarre-van de Waal HA. Cardiometabolic differences in children born after in vitro fertilization: follow-up study. The Journal of Clinical Endocrinology & Metabolism, 2008, 93(5): 1682-1688.

74. Chen M, Wu L, Zhao J, Wu F, Davies MJ, Wittert GA, Norman RJ, Robker RL, Heilbronn LK. Altered glucose metabolism in mouse and humans conceived by IVF. Diabetes, 2014, 63(10): 3189-3198.

75. Li B, Xiao X, Chen S, Huang J, Ma Y, Tang N, Sun H, Wang X. Changes of Phospholipids in Fetal Liver of Mice Conceived by In Vitro Fertilization. Biology of Reproduction, 2016, 94(5): E105.

76. Feuer SK, Donjacour A, Simbulan RK, Lin W, Liu X, Maltepe E, Rinaudo PF. Sexually dimorphic effect of in vitro fertilization (IVF) on adult mouse fat and liver metabolomes. Endocrinology, 2014, 155(11): 4554-4567.

77. Feuer S, Rinaudo P. From Embryos to Adults: A DOHaD Perspective on In Vitro Fertilization and Other Assisted Reproductive Technologies. Healthcare (Basel). 2016, 4(3): E51.

78. Wale PL, Gardner DK. The effects of chemical and physical factors on mammalian embryo culture and their importance for the practice of assisted human reproduction. Human Reproduction Update, 2016, 22(1):2-22.

79. Wang Y, Puscheck EE, Lewis JJ, Trostinskaia AB, Wang F, Rappolee DA. Increases in phosphorylation of SAPK/JNK and p38MAPK correlate negatively with mouse embryo development after culture in different media. Fertility and Sterility, 2005, 83(4): 1144-1154.

80. Hoeijmakers L, Kempe H, Verschure PJ. Epigenetic imprinting during assisted reproductive technologies: The effect of temporal and cumulative fluctuations in methionine cycling on the DNA methylation state. Molecular Reproduction and Development, 2016, 83(2): 94-107.

81. Giritharan G, Talbi S, Donjacour A, Di Sebastiano F, Dobson AT, Rinaudo PF. Effect of in vitro fertilization on gene expression and development of mouse preimplantation embryos. Reproduction, 2007, 134(1): 63-72.

82. Feuer SK, Liu X, Donjacour A, Lin W, Simbulan RK, Giritharan G, Piane LD, Kolahi K, Ameri K, Maltepe E, Rinaudo PF. Use of a mouse in vitro fertilization model to understand the developmental origins of health and disease hypothesis. Endocrinology, 2014, 155(5): 1956-1969.

83. DeBaun MR, Niemitz EL, Feinberg AP. Association of in vitro fertilization with Beckwith-Wiedemann syndrome and epigenetic alterations of LIT1 and H19. The American Journal of Human Genetics, 2003, 72(1): 156-160.

84. Ventura-Juncá P, Irarrázaval I, Rolle AJ, Gutiérrez JI, Moreno RD, Santos MJ. In vitro fertilization (IVF) in mammals: epigenetic and developmental alterations. Scientific and bioethical implications for IVF in humans. Biological research, 2015, 48(1): E68.

85. Nelissen EC, Dumoulin JC, Daunay A, Evers JL, Tost J, van Montfoort AP. Placentas from pregnancies conceived by IVF/ICSI have a reduced DNA methylation level at the H19 and MEST differentially methylated regions. Human Reproduction, 2013, 28(4):1117-1126.

86. Le F, Wang LY, Wang N, Li L, Li le J, Zheng YM, Lou HY, Liu XZ, Xu XR, Sheng JZ, Huang HF, Jin F. In vitro fertilization alters growth and expression of Igf2/H19 and their epigenetic mechanisms in the liver and skeletal muscle of newborn and elder mice. Biology of Reproduction, 2013, 88(3): E75.

87. Tan K, Wang X, Zhang Z, Miao K, Yu Y, An L, Tian J. Downregulation of miR-199a-5p Disrupts the Developmental Potential of In Vitro-Fertilized Mouse Blastocysts. Biology of Reproduction, 2016, 95(3): E54.

88. Ahima RS. Digging deeper into obesity. The Journal of Clinical Investigation, 2011, 121(6): 2076-2079.

89. Jacobs DR. Fast food and sedentary lifestyle: a combination that leads to obesity. The American Journal of Clinical Nutrition, 2006, 83(2): 189-190.

90. Muse ED, Obici S, Bhanot S, Monia BP, McKay RA, Rajala MW, Scherer PE, Rossetti L. Role of resistin in diet-induced hepatic insulin resistance. The Journal of Clinical Investigation, 2004, 114(2): 232-239.

91. Xu H1, Barnes GT, Yang Q, Tan G, Yang D, Chou CJ, Sole J, Nichols A, Ross JS, Tartaglia LA, Chen H. Chronic inflammation in fat plays a crucial role in the development of obesity-related insulin resistance. The Journal of Clinical Investigation, 2003, 112(12): 1821-1830.

92. Siersbæk R, Rabiee A, Nielsen R, Sidoli S, Traynor S, Loft A, La Cour Poulsen L, Rogowska-Wrzesinska A, Jensen ON, Mandrup S. Transcription factor cooperativity in early adipogenic hotspots and super-enhancers. Cell Reports, 2014, 7(5): 1443-1455.

93. Spiegelman BM, Flier JS. Obesity and the regulation of energy balance. Cell, 2001, 104(4): 531-543.

94 Chen Y, Siegel F, Kipschull S, Haas B, Fröhlich H, Meister G, Pfeifer A. miR-155 regulates differentiation of brown and beige adipocytes via a bistable circuit. Nature Communications, 2013, 4: 1769.

95. Fromme T, Klingenspor M. Uncoupling protein 1 expression and high-fat diets. American Journal of Physiology-Regulatory, Integrative and Comparative Physiology, 2011, 300(1): R1-8.

96. Feldmann HM1, Golozoubova V, Cannon B, Nedergaard J. UCP1 ablation induces obesity and abolishes diet-induced thermogenesis in mice exempt from thermal stress by living at thermoneutrality. Cell Metabolism, 2009, 9(2): 203-209.

97. Hensley K1, Robinson KA, Gabbita SP, Salsman S, Floyd RA. Reactive oxygen species, cell signaling, and cell injury. Free Radical Biology and Medicine, 2000, 28(10): 1456-1462.

98. Hui X, Gu P, Zhang J, Nie T, Pan Y, Wu D, Feng T, Zhong C, Wang Y, Lam KS, Xu A. Adiponectin enhances cold-induced browning of subcutaneous adipose

tissue via promoting M2 macrophage proliferation. Cell Metabolism, 2015, 22(2): 279-290.

99. Rao RR, Long JZ, White JP, Svensson KJ, Lou J, Lokurkar I, Jedrychowski MP, Ruas JL, Wrann CD, Lo JC, Camera DM, Lachey J, Gygi S, Seehra J, Hawley JA, Spiegelman BM. Meteorin-like is a hormone that regulates immune-adipose interactions to increase beige fat thermogenesis. Cell, 2014, 157(6): 1279-1291.
100. Smyth, GK. in Bioinformatics and Computational Biology Solutions Using R and Bioconductor. Springer Science & Business Media, 2005, 397–420.
101. Kanehisa M1, Goto S, Sato Y, Kawashima M, Furumichi M, Tanabe M. Data, information, knowledge and principle: back to metabolism in KEGG. Nucleic Acids Research, 2014, 42(D1): 199-205.
102. Guerin P, El Mouatassim S, Menezo Y. Oxidative stress and protection against reactive oxygen species in the pre-implantation embryo and its surroundings. Human Reproduction Update, 2001, 7(2): 175-189.
103. De Matos DG, Furnus CC. The importance of having high glutathione (GSH) level after bovine in vitro maturation on embryo development: effect of β-mercaptoethanol, cysteine and cystine. Theriogenology, 2000, 53(3): 761-771.
104. Ito K, Hirao A, Arai F, Takubo K, Matsuoka S, Miyamoto K, Ohmura M, Naka K, Hosokawa K, Ikeda Y, Suda T. Reactive oxygen species act through p38 MAPK to limit the lifespan of hematopoietic stem cells. Nature Medicine, 2006, 12(4): 446-451.
105. Ricklin D, Hajishengallis G, Yang K, Lambris JD. Complement: a key system for immune surveillance and homeostasis. Nature Immunology, 2010, 11(9): 785-797.

106. Xiao M, Yang H, Xu W, Ma S, Lin H, Zhu H, Liu L, Liu Y, Yang C, Xu Y, Zhao S, Ye D, Xiong Y, Guan KL. Inhibition of α-KG-dependent histone and DNA demethylases by fumarate and succinate that are accumulated in mutations of FH and SDH tumor suppressors. Genes & Development, 2012, 26(12): 1326-1338.

Figure legends

Figure 1-1. The structure of members of ATF2 family of transcription factors and the function of ATF7 as a transcriptional repressor.

A) The protein structure of three members of ATF2 family of transcription factors. stress-activated protein kinase (SAPK) phosphorylation sites of ATF2 and ATF7 are marked in red. TAD: *trans*-activation domain; bZIP: basic leucine zipper domain. **B)** The ATF7 acts as the transcriptional repressor in brain and macrophage via recruitment of the histone H3K9 trimethyltransferase ESET or the histone H3K9 dimethyltransferase G9a, respectively.

Figure 1-2. The transcriptional regulation of development and thermogenic function of adipocytes.

A) The development of brown adipocyte. **B)** The development of beige and white adipocytes. The dot-dashed line repents the controversial origins of beige cells. **C)** The induction of thermogenic gene program in beige/brown adipocytes by various endocrine factors released from related organs and cells. The key transcriptional factors controlling the express of thermogenic genes are shown.

Figure 2-1. ATF7-deficient mice exhibited resistance to obesity.

A) A representative photograph of 5-month-old wild-type (WT, left) and *Atf7*$^{-/-}$ (right) mice. **B)** Body weight of *Atf7*$^{-/-}$ and WT littermates fed on a standard chow diet (CD) or a high-fat diet (HFD) (n = 8–9 for each group). **C)** Serum

cholesterol levels in WT and *Atf7*$^{-/-}$ mice (n = 4–7 for each group). **D)** Serum triglycerides levels in WT and *Atf7*$^{-/-}$ mice (n = 4–7 for each group). *, P < 0.05, **, P < 0.01, ***, P < 0.001, NS, not significant.

Figure 2-2. Reduction in adipose tissue mass in *Atf7*$^{-/-}$ mice.

A) Body fat percentage in 5-month-old WT and *Atf7*$^{-/-}$ mice fed on a CD or a HFD (n = 8–9 for each group). **B)** Masses of epididymal white adipose tissue (eWAT), inguinal white adipose tissue (iWAT), brown adipose tissue (BAT), and liver relative to total body mass (n = 6 for each group). **C)** Histological analysis of eWAT using H&E staining. Bar = 50 μm. **D)** Serum resistin levels in 4-month-old WT and *Atf7*$^{-/-}$ mice (n = 4–7 for each group). *, P < 0.05, **, P < 0.01, ***, P < 0.001, NS, not significant.

Figure 2-3. ATF7 deficiency improved insulin sensitivity.

A) Serum insulin levels in 4-month-old WT and *Atf7*$^{-/-}$ mice (n = 4–7 for each group). **B)** Serum fasting glucose levels in 4-month-old WT and *Atf7*$^{-/-}$ mice (n = 4–7 for each group). **C)** Glucose tolerance test in WT and *Atf7*$^{-/-}$ mice on a CD and **D)** HFD (n = 6 for each group). **E)** Insulin tolerance test in WT and *Atf7*$^{-/-}$ mice on a CD and **F)** HFD (n = 6 for each group). *, *P* < 0.05, **, *P* < 0.01, ***, *P* < 0.001, NS, not significant.

Figure 2-4. Higher energy expenditure in *Atf7*$^{-/-}$ mice on a HFD.

A) Food intake of 12-week-old WT and *Atf7*$^{-/-}$ mice on a CD or a HFD (n = 5 for each group). **B and C)** Oxygen consumption in 12-week-old WT and *Atf7*$^{-/-}$ mice on a CD (n = 7 for each group). **D and E)** Oxygen consumption in 12-week-old WT and *Atf7*$^{-/-}$ mice on a HFD (n = 7 for each group). **, $P < 0.01$, ***, $P < 0.001$, NS, not significant.

Figure 2-5. The involvement of ATF7 in the thermogenic gene program.

A) Protein expression level of ATF7 in adipose tissues. **B)** UCP1 expression level of WT and *Atf7*$^{-/-}$ BAT and iWAT. **C)** H&E staining and immunohistostaining of UCP1 of WT and *Atf7*$^{-/-}$ iWAT. **D)** The overlap of up-regulated genes induced by cold exposure for one week (number GEO for dataset :GSE13432） and up-regulated genes in *Atf7*$^{-/-}$ iWAT compared with that of WT. Statistical significance of the overlap was examined by Fisher's exact test. The gene names of top 20 in the list of up-regulated genes in *Atf7*$^{-/-}$ iWAT and genes which are also induced by cold exposure are marked in red. **E)** The phosphorylation level of ATF7 of BAT in presence/absence of cold exposure for one hour. **F)** UCP1 expression level of WT and *Atf7*$^{-/-}$ BAT after 24 h cold exposure.

Figure 2-6. ATF7 is required for adipogenesis.

A) The mRNA expression level of ATF7 in stromal vascular fraction (SVF) cells and mature adipocytes of BAT and iWAT (n=3). P value: (paired student's t-test) NS >0.05 **B)** The adipocytes differentiation of WT and *Atf7*$^{-/-}$ iWAT SVF cells. The red oil O staining of differentiated adipocytes was shown. **C)** The mRNA expression level of the key transcription factors in differentiated adipocytes inducted from iWAT SVF cells (n=3). Bars are means + s.e.m. P value: (paired student's t-test) **, < 0.01, ***, < 0.001. **D)** The adipocytes differentiation of C3H10T1/2 cells expressing dsRed or Flag-ATF7. The red oil O staining of differentiated adipocytes was shown. **E)** The mRNA expression level of the key transcription factors in cells after 2 days cultured in the induction medium(n=3). Bars are means + s.e.m. P value: (paired student's t-test) *, < 0.05, ***, < 0.001, NS, >0.05.

Figure 3-1. Effects of IVF on gene expression pattern in liver.

A) Volcano plot for the analysis of differential gene expression between IVF and natural mating samples. IVF up-regulated 668 genes (yellow spots) and down-regulated 204 genes (blue spots). The data point for *Mest* is marked with an asterisk. **B** and **C)** KEGG pathway enrichment analysis was performed for genes up- and down-regulated by IVF, respectively. P-values for the gene enrichment analysis were calculated by a modified Fisher's exact test, and the number to the right of each bar is the number of genes involved in each pathway. Thirteen KEGG pathways (P < 0.1) were over-represented among up-regulated genes, and five of these were

associated with metabolism (in red) (B). Seven KEGG pathways (P < 0.1) were over-represented among down-regulated genes (C). **D)** Gene expression of *Mest* in natural mating and IVF samples (n = 3). Bars are means + s.e.m. P-value: (paired Student's t-test) ***, < 0.001.

Figure 3-2. Ablation of ATF7 reduces the effects of IVF on gene expression in liver.

A) The levels of *Atf7* mRNA in liver of naturally and IVF-derived mice. Bars are means + s.e.m. P-value: (paired Student's t-test) NS, > 0.05. **B)** ATF7 protein levels in liver of naturally and IVF-derived mice were examined by western blotting. *Atf7*$^{-/-}$ mice were used as a negative control, and tubulin was the loading control. **C)** Volcano plot for the analysis of differential gene expression between *Atf7*$^{-/-}$ IVF and *Atf7*$^{-/-}$ natural mating samples. IVF up-regulated 508 genes (yellow spots) and down-regulated 825 genes (blue spots). **D)** Venn diagram showing overlap in IVF-induced up-regulated genes between WT and *Atf7*$^{-/-}$ livers. Statistical significance of the overlap was examined by Fisher's exact test. **E)** KEGG pathway enrichment analysis for IVF-induced up-regulated genes in *Atf7*$^{-/-}$ mice. P-values for the gene enrichment analysis were calculated by a modified Fisher's exact test, and the number to the right of each bar is the number of genes involved in each pathway. Thirteen KEGG pathways (P < 0.1) were over-represented among up-regulated genes, and five pathways were common with those over-represented among IVF-induced up-regulated genes in WT mice (marked by asterisks).

Figure 3-3. ATF7 deficiency partially mimics the effects of IVF on gene expression in liver.

A) Volcano plot for the analysis of differential gene expression between *Atf7*$^{-/-}$ and WT samples. Loss of ATF7 resulted in up-regulation of 903 genes (yellow spots) and down-regulation of 416 genes (blue spots). **B)** Venn diagram showing overlap between IVF-induced and ATF7 deficiency-induced up-regulated genes. Statistical significance of the overlap was examined by Fisher's exact test. **C)** KEGG pathway enrichment analysis for ATF7 deficiency-induced up-regulated genes. P-values for the gene enrichment analysis were calculated by a modified Fisher's exact test, and the number to the right of each bar is the number of genes involved in each pathway. Seventeen KEGG pathways ($P < 0.1$) were over-represented among up-regulated genes, and six pathways were common with those over-represented among IVF-induced up-regulated genes in WT mice (marked by asterisks). **D)** Unsupervised hierarchical clustering using IVF-induced differential gene expression between IVF and natural mating samples. Red and green indicate higher and lower expression levels, respectively.

Figure 3-4. Involvement of ATF7 in the effect of IVF on metabolic pathways.

A) Heat map for expression profile of genes involved in purine metabolism. Red and green indicate higher and lower expression levels, respectively. **B)** The expression levels of *Nt5e* in four groups of samples (n = 3). Bars are means + s.e.m. P-value: (paired Student's t-test) *, < 0.05, ***, < 0.001. **C)** Heat map for expression profile of genes involved in terpenoid backbone biosynthesis. Red and green indicate higher and lower expression levels, respectively. **D)** The expression levels of *Idi1* in four groups of samples (n = 3). Bars are means + s.e.m. P-value: (paired Student's t-test) *, < 0.05, ***, < 0.001. **E)** The potential role of ATF7 in IVF-induced gene expression changes.

Figures

Figure 1-1.

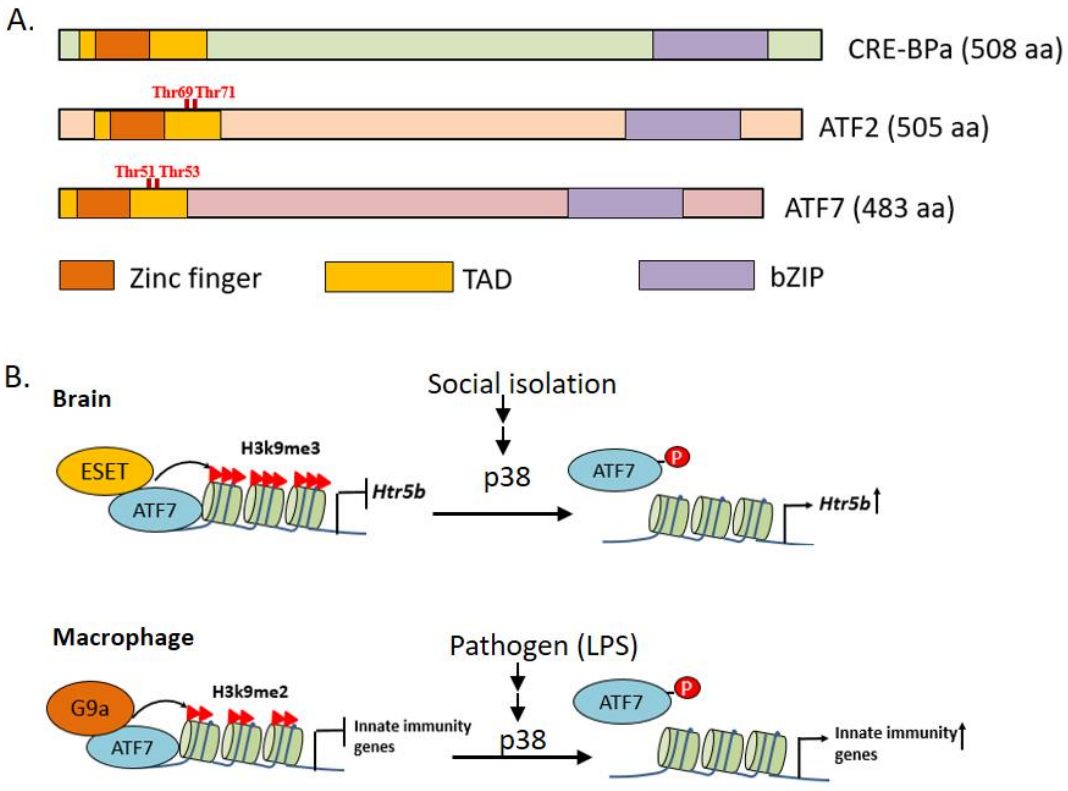

Figure 1-2.

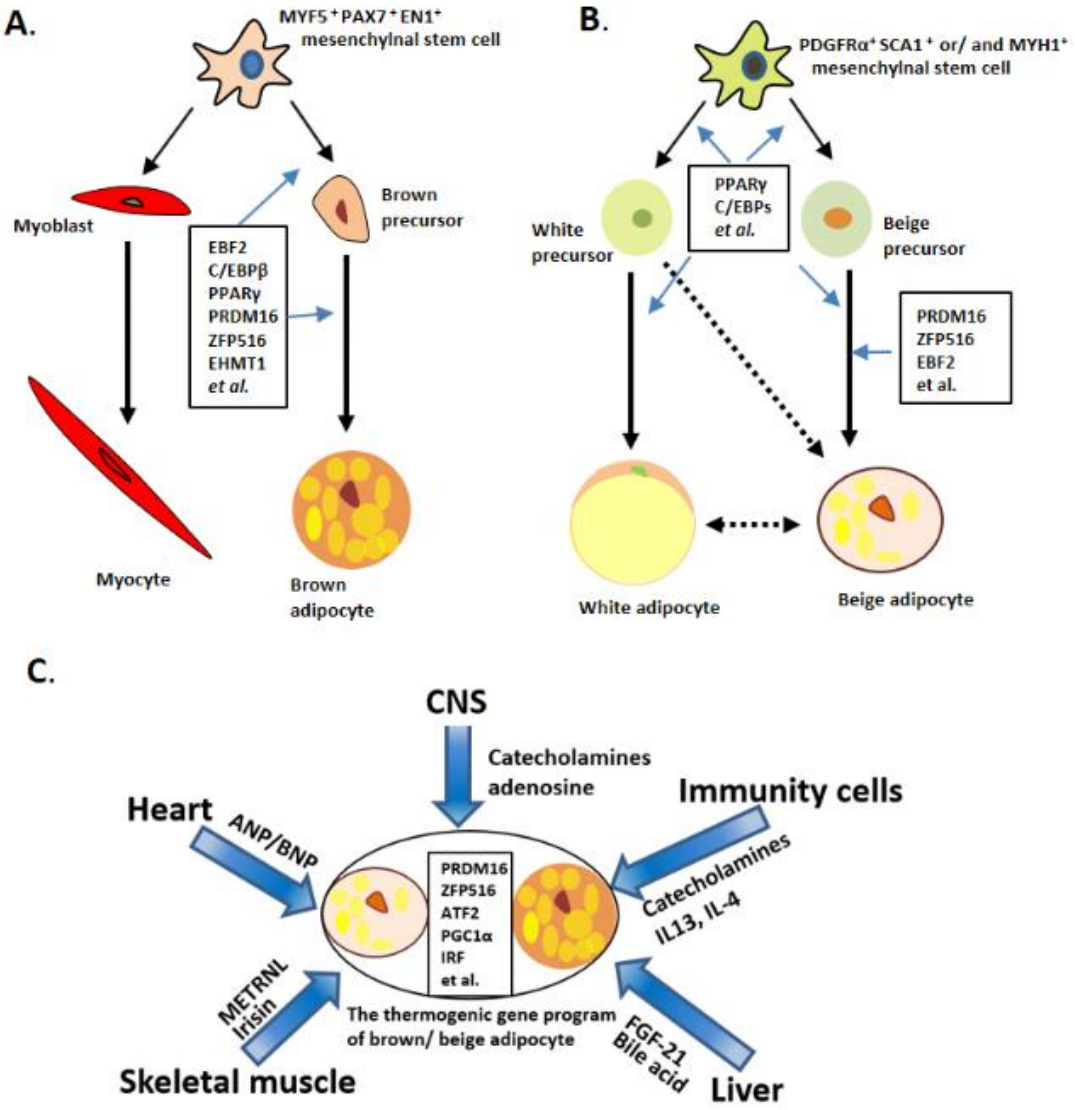
A.
MYF5+PAX7+EN1+
mesenchylnal stem cell
Myoblast
Brown
precursor
EBF2
C/EBPβ
PPARγ
PRDM16
ZFP516
EHMT1
et al.
Myocyte
Brown
adipocyte
B.
PDGFRα+SCA1+ or/ and MYH1+
mesenchylnal stem cell
PPARγ
C/EBPs
et al.
White
precursor
Beige
precursor
PRDM16
ZFP516
EBF2
et al.
White adipocyte
Beige adipocyte
C.
CNS
Catecholamines
adenosine
Heart
ANP/BNP
Immunity cells
Catecholamines
IL13, IL-4
PRDM16
ZFP516
ATF2
PGC1α
IRF
et al.
METRNL
Irisin
The thermogenic gene program
of brown/ beige adipocyte
FGF-21
Bile acid
Skeletal muscle
Liver

Figure 2-1.

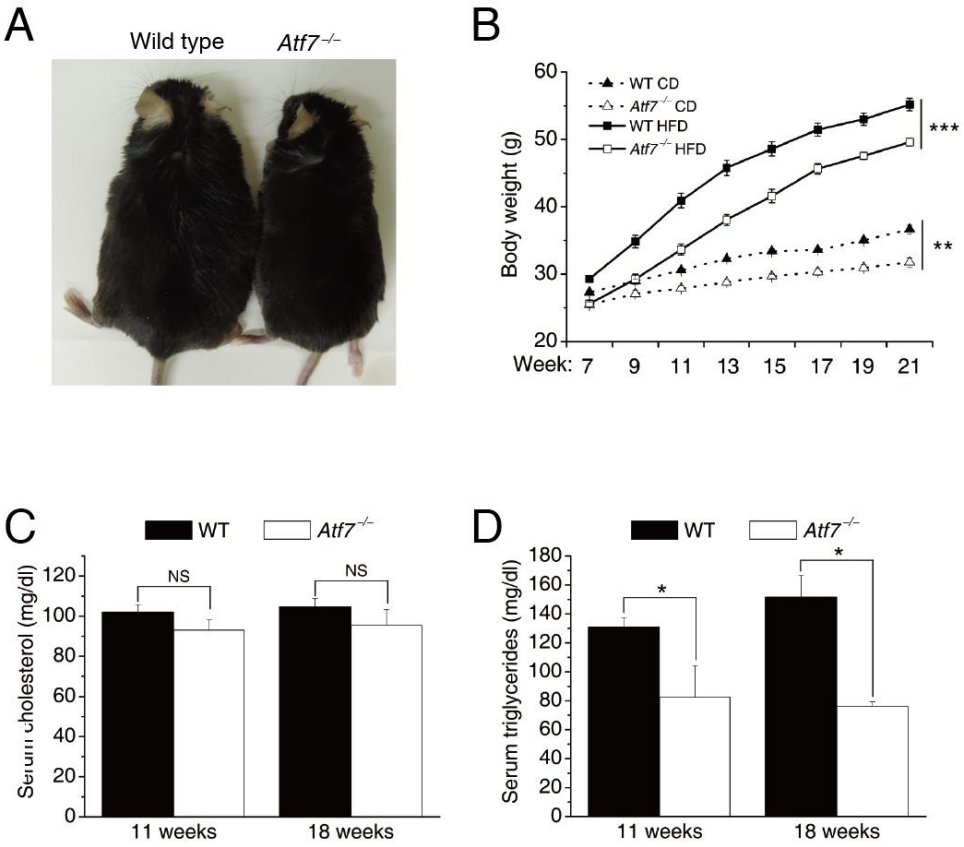
A
Wild type
Atf7-/-
B
WT CD
Atf7-/- CD
WT HFD
Atf7-/- HFD
Body weight (g)
Week: 7 9 11 13 15 17 19 21
***
**
C
WT
Atf7-/-
Serum cholesterol (mg/dl)
NS
NS
11 weeks
18 weeks
D
WT
Atf7-/-
Serum triglycerides (mg/dl)
*
*
11 weeks
18 weeks

Figure 2-2.

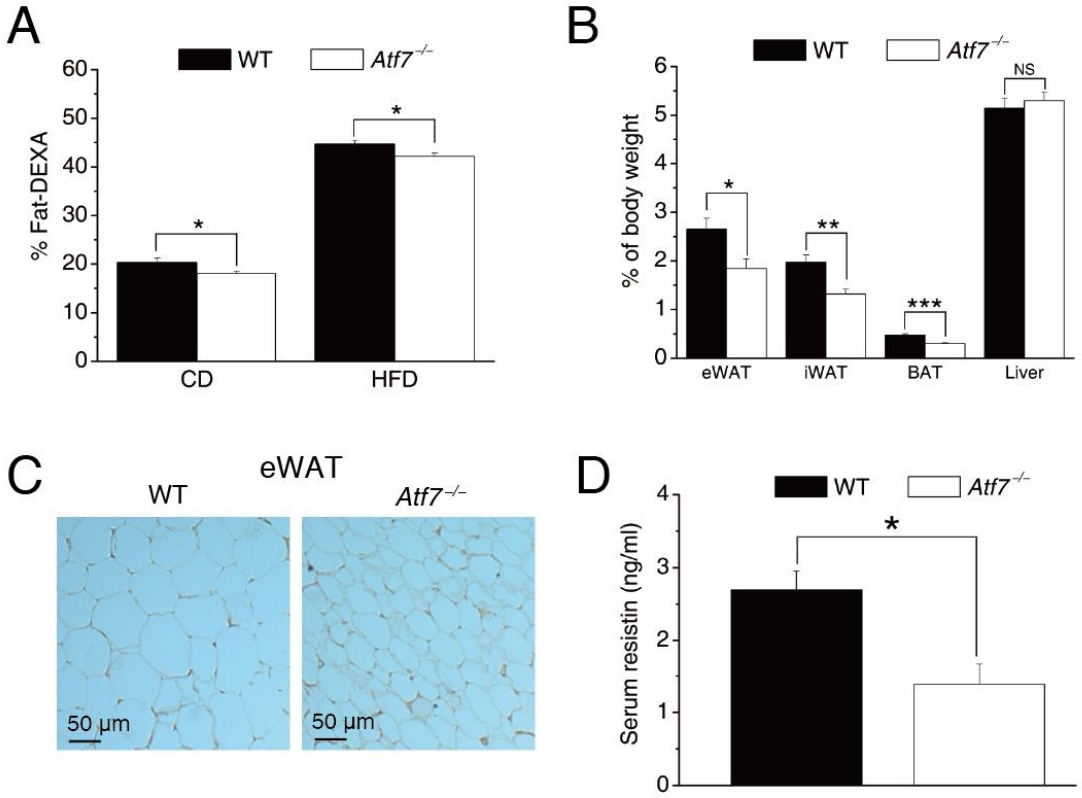
A
WT
Atf7-/-
% Fat-DEXA
60
50
40
30
20
10
0
*
*
CD
HFD
B
WT
Atf7-/-
NS
% of body weight
6
5
4
3
2
1
0
*
**
***
eWAT
iWAT
BAT
Liver
C
eWAT
WT
Atf7-/-
50 μm
50 μm
D
WT
Atf7-/-
Serum resistin (ng/ml)
4
3
2
1
0
*

Figure 2-3

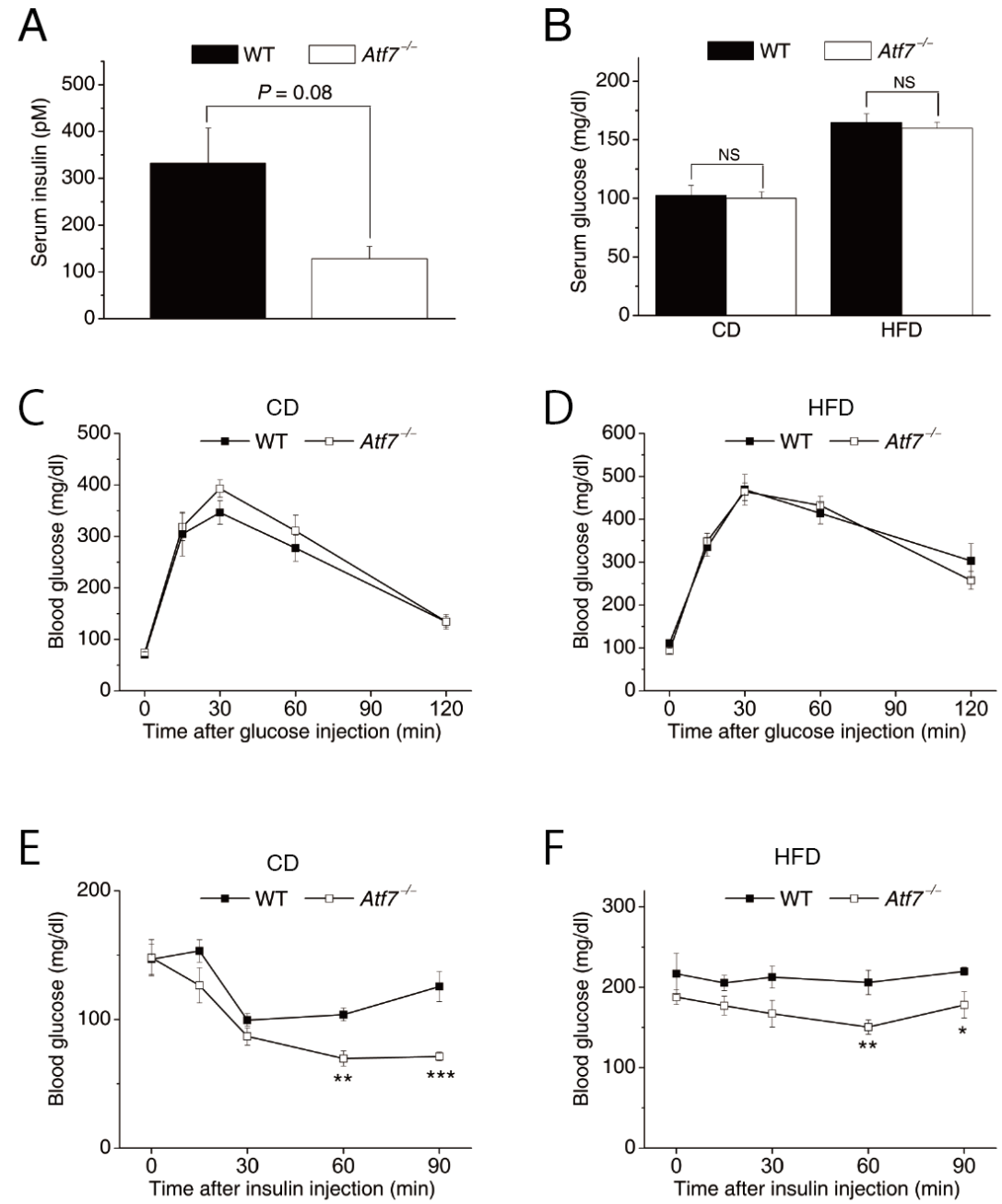
A
WT
Atf7-/-
P = 0.08
Serum insulin (pM)
500
400
300
200
100
0
B
WT
Atf7-/-
NS
NS
Serum glucose (mg/dl)
200
150
100
50
0
CD
HFD
C
CD
WT
Atf7-/-
Blood glucose (mg/dl)
500
400
300
200
100
0
0
30
60
90
120
Time after glucose injection (min)
D
HFD
WT
Atf7-/-
Blood glucose (mg/dl)
600
500
400
300
200
100
0
0
30
60
90
120
Time after glucose injection (min)
E
CD
WT
Atf7-/-
Blood glucose (mg/dl)
200
100
0
**
***
0
30
60
90
Time after insulin injection (min)
F
HFD
WT
Atf7-/-
Blood glucose (mg/dl)
300
200
100
0
**
*
0
30
60
90
Time after insulin injection (min)

Figure 2-4.

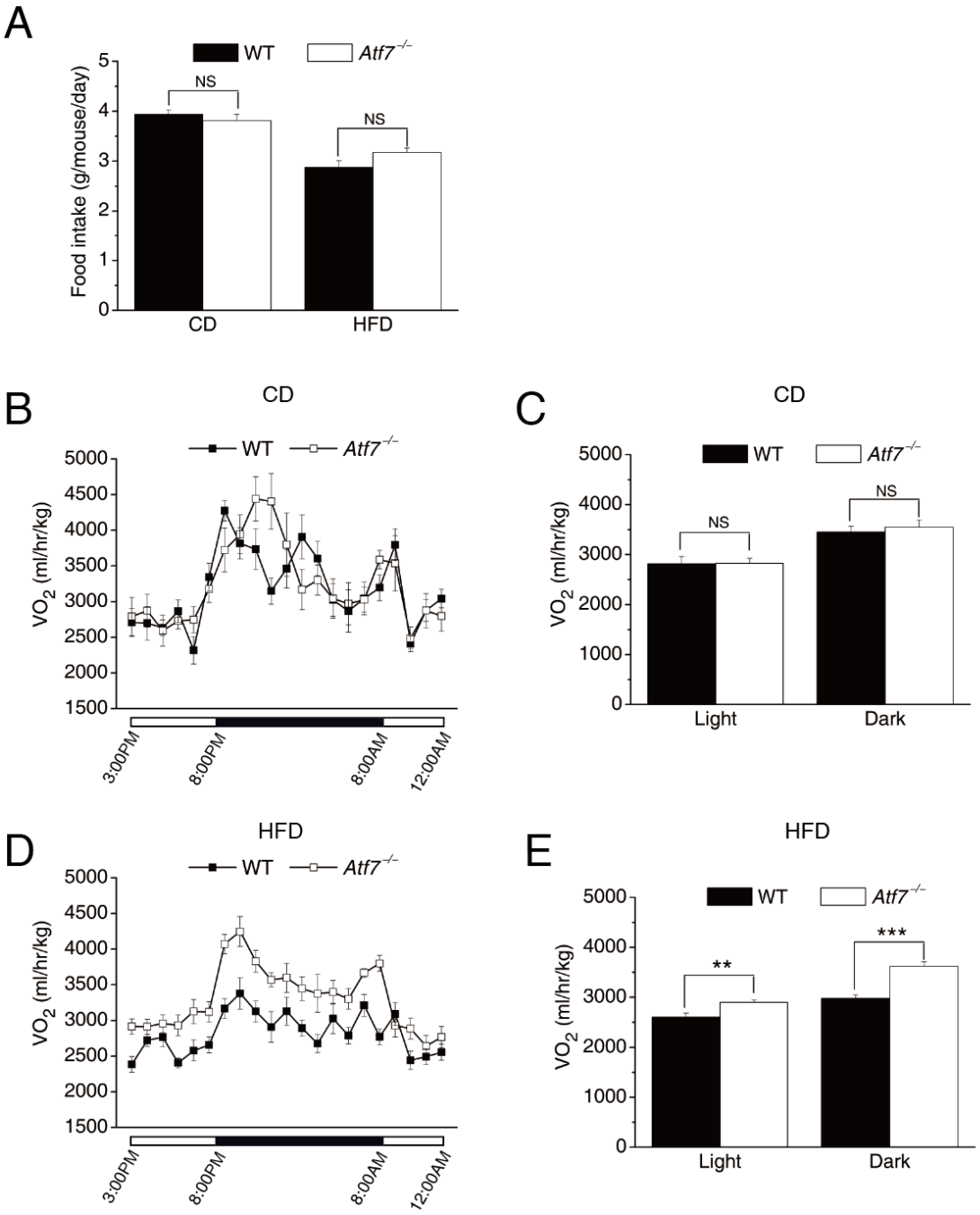
A
WT
Atf7-/-
Food intake (g/mouse/day)
NS
NS
CD
HFD
B
CD
WT
Atf7-/-
VO2 (ml/hr/kg)
3:00PM
8:00PM
8:00AM
12:00AM
C
CD
WT
Atf7-/-
NS
NS
VO2 (ml/hr/kg)
Light
Dark
D
HFD
WT
Atf7-/-
VO2 (ml/hr/kg)
3:00PM
8:00PM
8:00AM
12:00AM
E
HFD
WT
Atf7-/-
**
***
VO2 (ml/hr/kg)
Light
Dark

Figure 2-5.

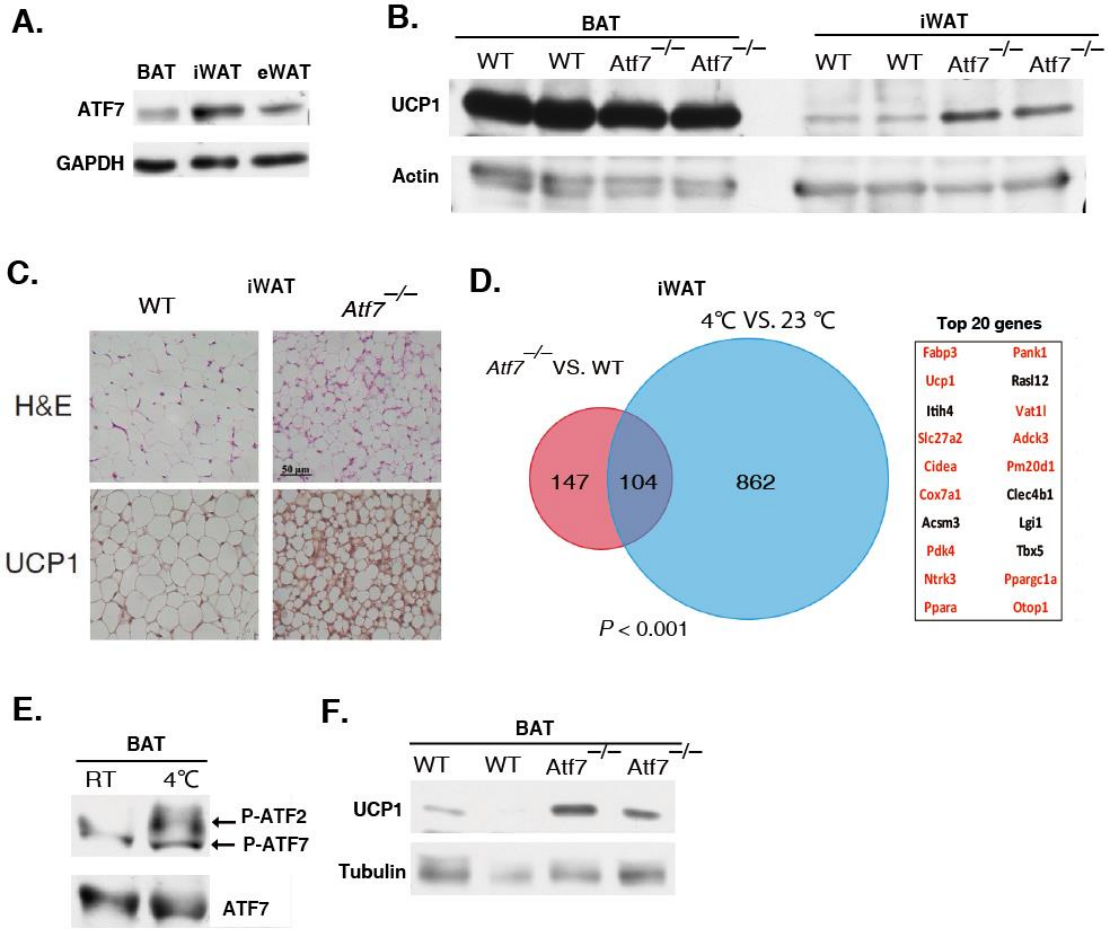
A.
BAT iWAT eWAT
ATF7
GAPDH
B.
BAT
iWAT
WT WT Atf7−/− Atf7−/−
WT WT Atf7−/− Atf7−/−
UCP1
Actin
C.
WT
iWAT
Atf7−/−
H&E
UCP1
50 μm
D.
iWAT
4℃ VS. 23 ℃
Atf7−/− VS. WT
147
104
862
P < 0.001
Top 20 genes
Fabp3 Pank1
Ucp1 Rasl12
Itih4 Vat1l
Slc27a2 Adck3
Cidea Pm20d1
Cox7a1 Clec4b1
Acsm3 Lgi1
Pdk4 Tbx5
Ntrk3 Ppargc1a
Ppara Otop1
E.
BAT
RT 4℃
P-ATF2
P-ATF7
ATF7
F.
BAT
WT WT Atf7−/− Atf7−/−
UCP1
Tubulin

Figure 2-6.

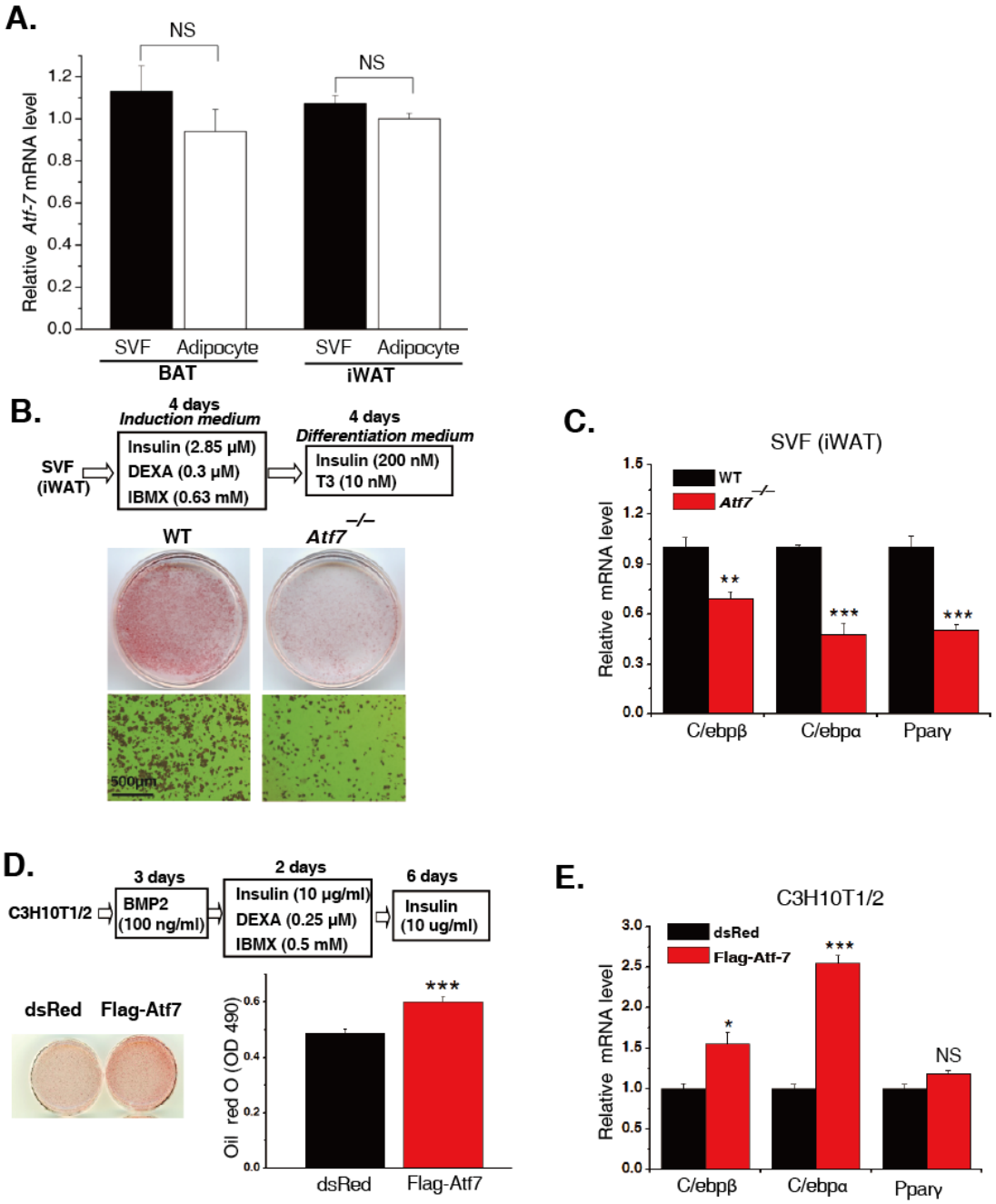
A.
NS
NS
Relative Atf-7 mRNA level
1.2
1.0
0.8
0.6
0.4
0.2
0.0
SVF
Adipocyte
SVF
Adipocyte
BAT
iWAT
B.
4 days
Induction medium
Insulin (2.85 μM)
DEXA (0.3 μM)
IBMX (0.63 mM)
4 days
Differentiation medium
Insulin (200 nM)
T3 (10 nM)
SVF (iWAT)
WT
Atf7 −/−
500μm
C.
SVF (iWAT)
WT
Atf7 −/−
Relative mRNA level
1.5
1.2
0.9
0.6
0.3
0.0
**
***
***
C/ebpβ
C/ebpα
Pparγ
D.
3 days
2 days
6 days
C3H10T1/2
BMP2 (100 ng/ml)
Insulin (10 μg/ml)
DEXA (0.25 μM)
IBMX (0.5 mM)
Insulin (10 ug/ml)
dsRed
Flag-Atf7
Oil red O (OD 490)
0.6
0.4
0.2
0.0
***
dsRed
Flag-Atf7
E.
C3H10T1/2
dsRed
Flag-Atf-7
Relative mRNA level
3.0
2.5
2.0
1.5
1.0
0.5
0.0
*
***
NS
C/ebpβ
C/ebpα
Pparγ

Figure 3-1.

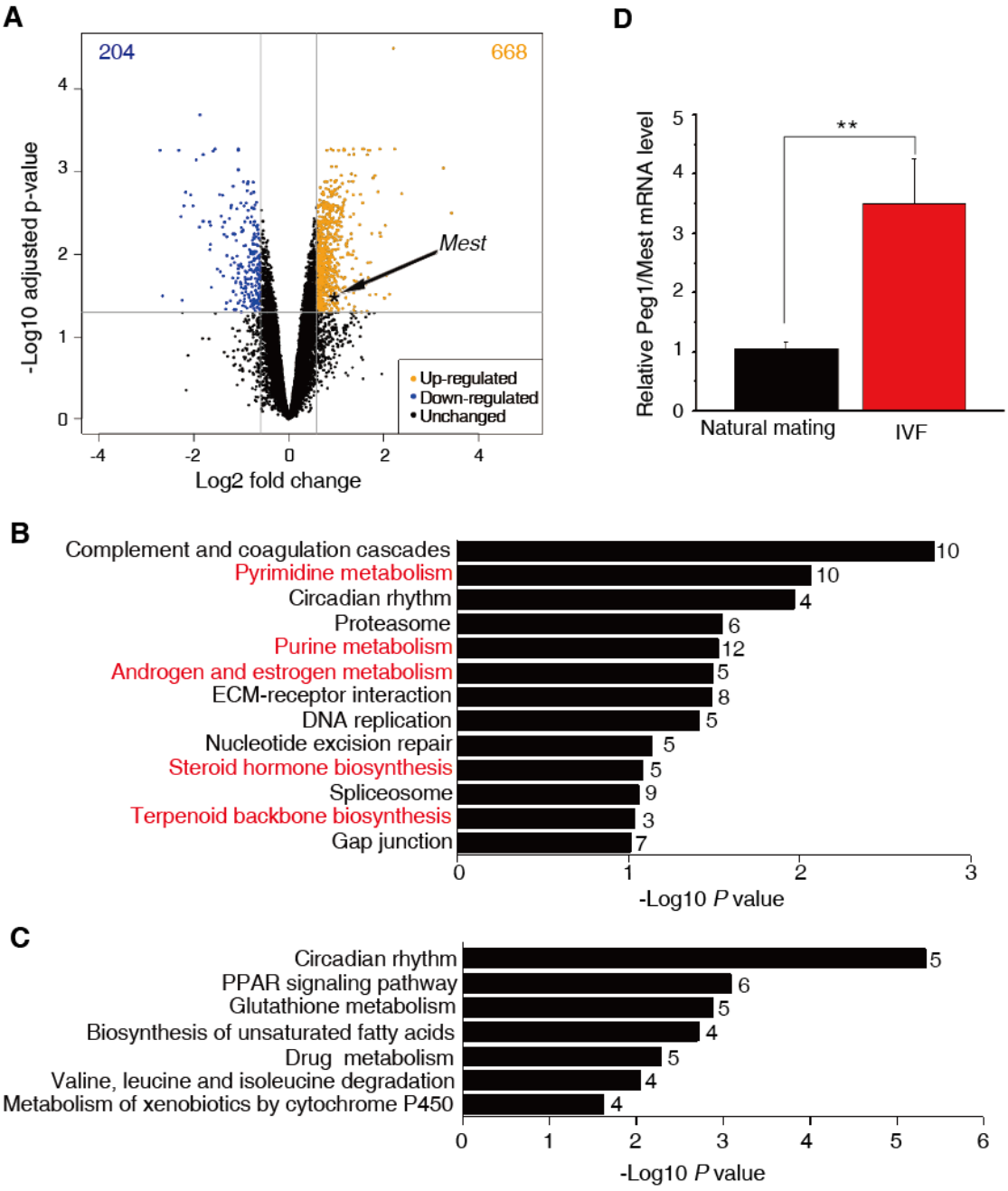
A
204
668
Mest
Up-regulated
Down-regulated
Unchanged
-Log10 adjusted p-value
Log2 fold change
D
Relative Peg1/Mest mRNA level
**
Natural mating
IVF
B
Complement and coagulation cascades 10
Pyrimidine metabolism 10
Circadian rhythm 4
Proteasome 6
Purine metabolism 12
Androgen and estrogen metabolism 5
ECM-receptor interaction 8
DNA replication 5
Nucleotide excision repair 5
Steroid hormone biosynthesis 5
Spliceosome 9
Terpenoid backbone biosynthesis 3
Gap junction 7
-Log10 P value
C
Circadian rhythm 5
PPAR signaling pathway 6
Glutathione metabolism 5
Biosynthesis of unsaturated fatty acids 4
Drug metabolism 5
Valine, leucine and isoleucine degradation 4
Metabolism of xenobiotics by cytochrome P450 4
-Log10 P value

Figure 3-2.

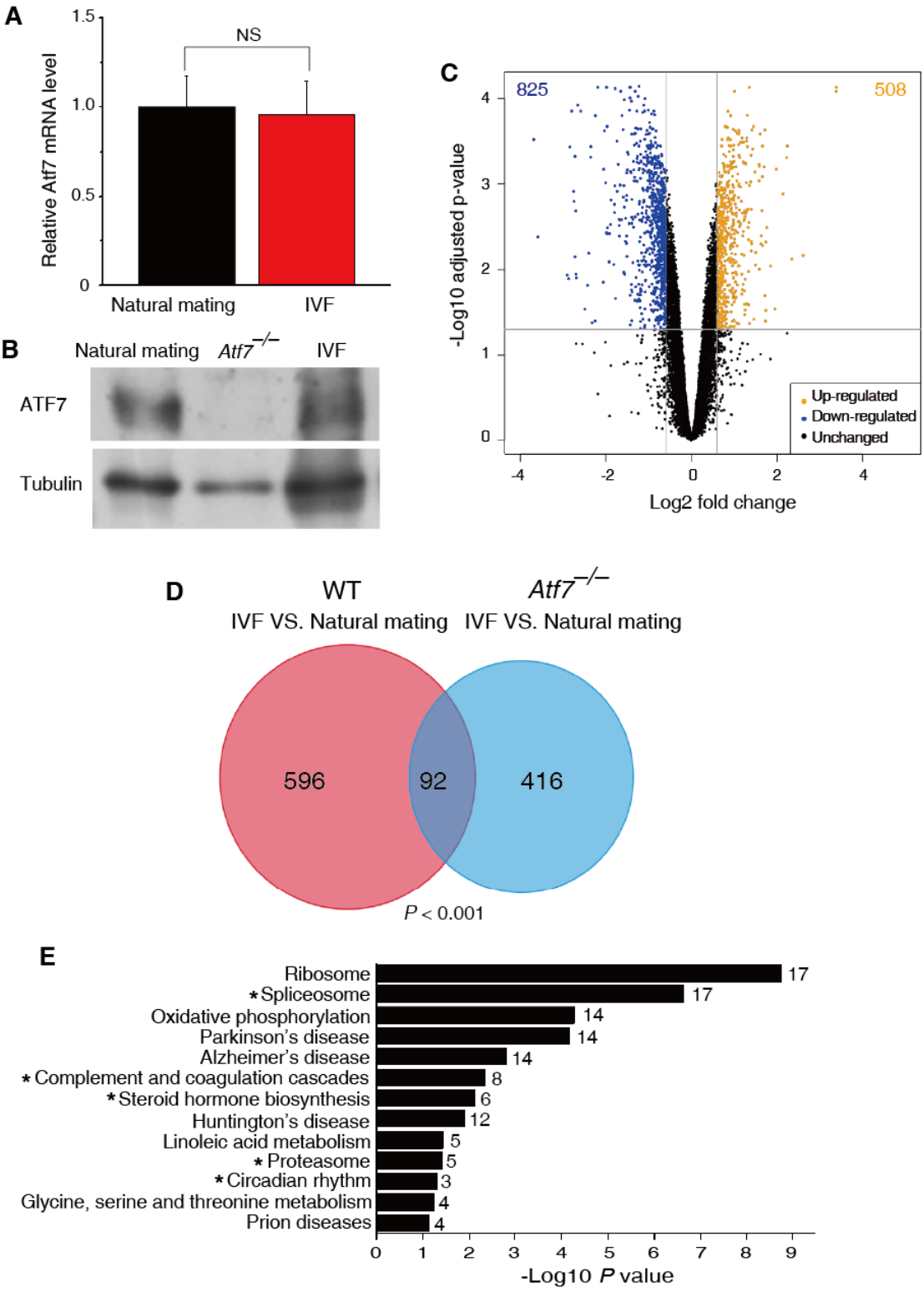
A
Relative Atf7 mRNA level
1.5
1.0
0.5
0
NS
Natural mating
IVF
B
Natural mating
Atf7−/−
IVF
ATF7
Tubulin
C
825
508
-Log10 adjusted p-value
Log2 fold change
Up-regulated
Down-regulated
Unchanged
D
WT
IVF VS. Natural mating
Atf7−/−
IVF VS. Natural mating
596
92
416
P < 0.001
E
Ribosome 17
*Spliceosome 17
Oxidative phosphorylation 14
Parkinson's disease 14
Alzheimer's disease 14
*Complement and coagulation cascades 8
*Steroid hormone biosynthesis 6
Huntington's disease 12
Linoleic acid metabolism 5
*Proteasome 5
*Circadian rhythm 3
Glycine, serine and threonine metabolism 4
Prion diseases 4
-Log10 P value

Figure 3-3.

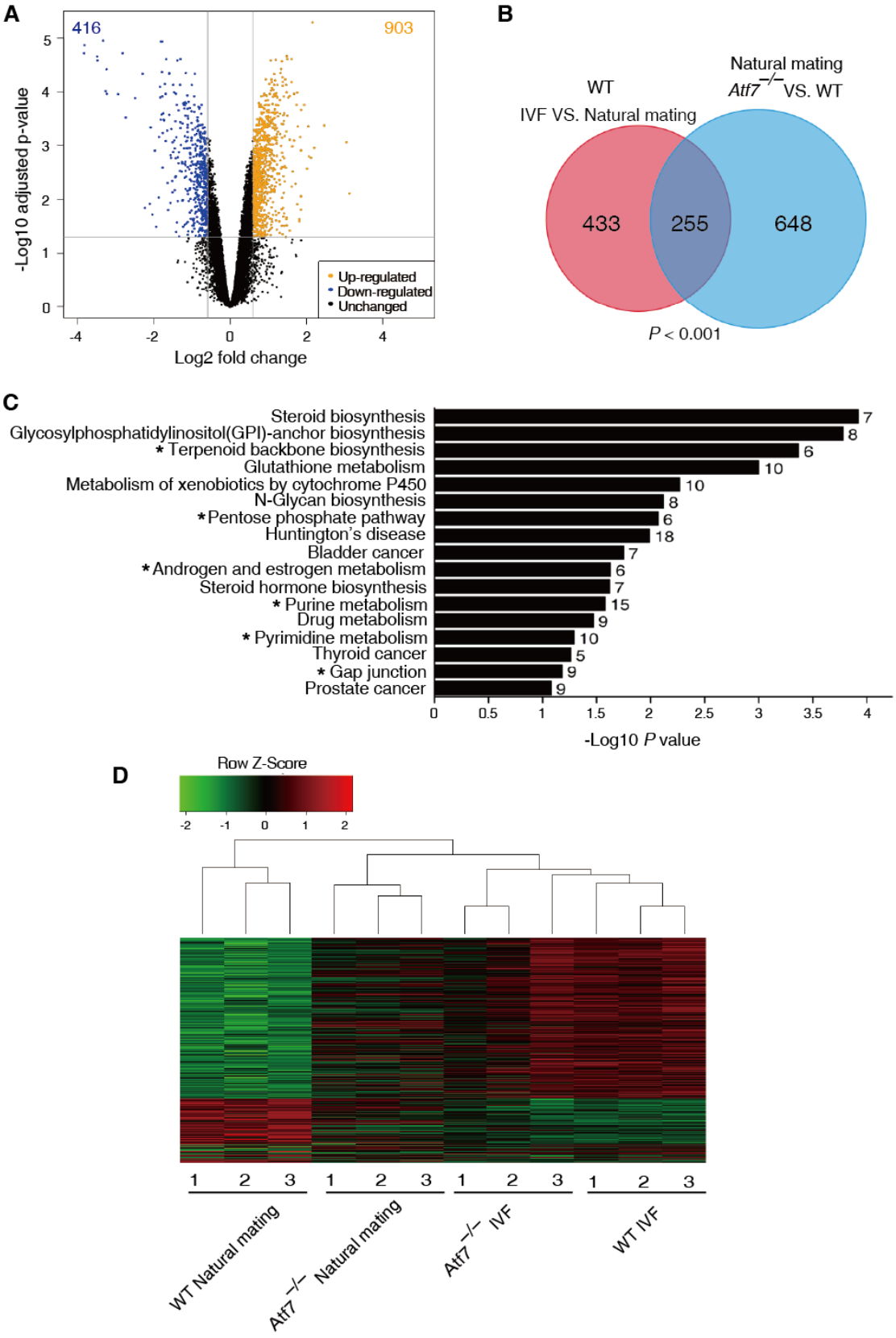
A
416
903
-Log10 adjusted p-value
Log2 fold change
Up-regulated
Down-regulated
Unchanged
B
WT
IVF VS. Natural mating
Natural mating
Atf7−/− VS. WT
433
255
648
P < 0.001
C
Steroid biosynthesis 7
Glycosylphosphatidylinositol(GPI)-anchor biosynthesis 8
* Terpenoid backbone biosynthesis 6
Glutathione metabolism 10
Metabolism of xenobiotics by cytochrome P450 10
N-Glycan biosynthesis 8
* Pentose phosphate pathway 6
Huntington's disease 18
Bladder cancer 7
* Androgen and estrogen metabolism 6
Steroid hormone biosynthesis 7
* Purine metabolism 15
Drug metabolism 9
* Pyrimidine metabolism 10
Thyroid cancer 5
* Gap junction 9
Prostate cancer 9
-Log10 P value
D
Row Z-Score
WT Natural mating
Atf7−/− Natural mating
Atf7−/− IVF
WT IVF

Figure 3-4.

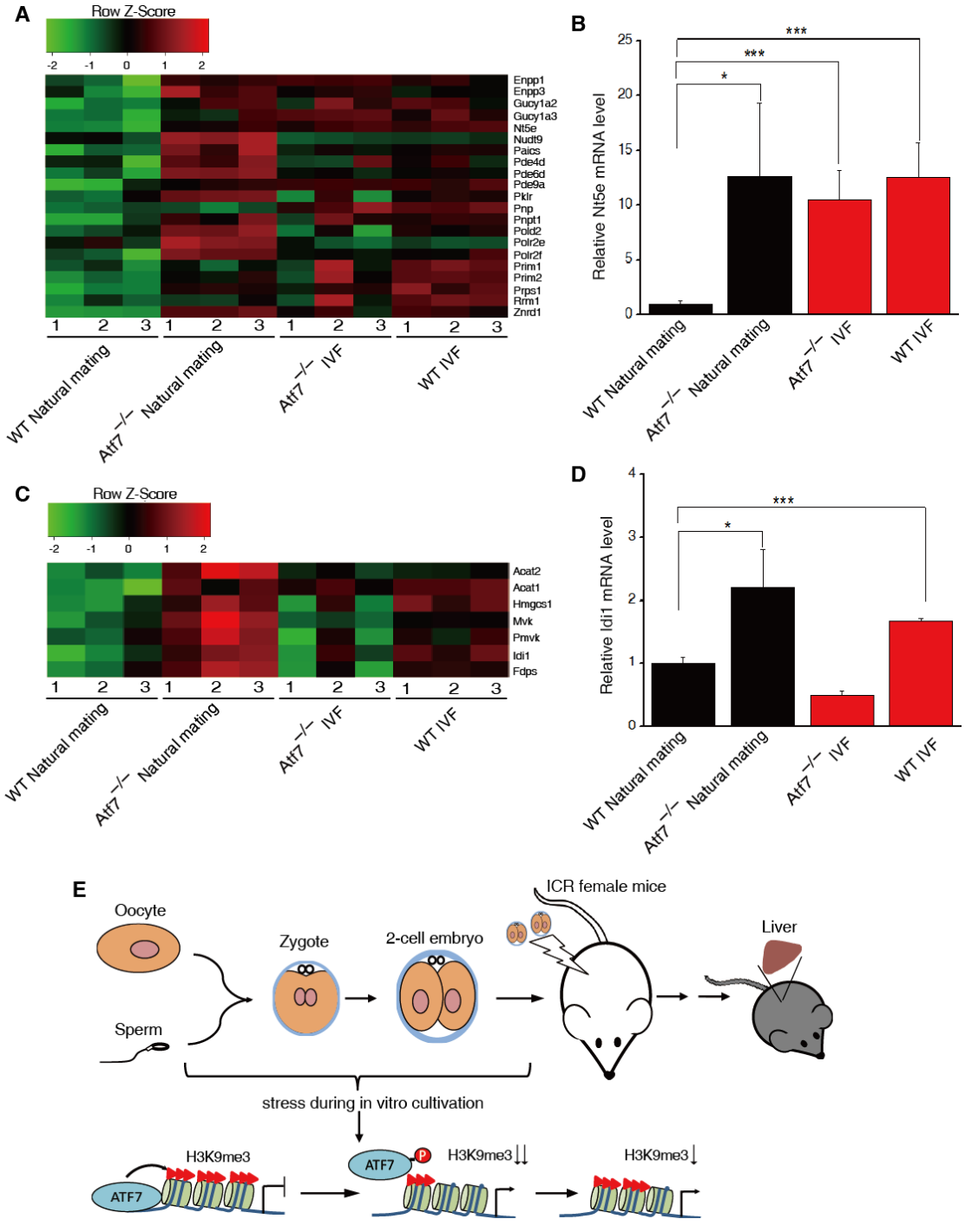
A
Row Z-Score
-2 -1 0 1 2
Enpp1
Enpp3
Gucy1a2
Gucy1a3
Nt5e
Nudt9
Paics
Pde4d
Pde6d
Pde9a
Pklr
Pnp
Pngt1
Pold2
Polr2e
Polr2f
Prim1
Prim2
Prps1
Rrm1
Znrd1
1 2 3 1 2 3 1 2 3 1 2 3
WT Natural mating
Atf7 −/− Natural mating
Atf7 −/− IVF
WT IVF
B
Relative Nt5e mRNA level
25
20
15
10
5
0
***
***
*
WT Natural mating
Atf7 −/− Natural mating
Atf7 −/− IVF
WT IVF
C
Row Z-Score
-2 -1 0 1 2
Acat2
Acat1
Hmgcs1
Mvk
Pmvk
Idi1
Fdps
1 2 3 1 2 3 1 2 3 1 2 3
WT Natural mating
Atf7 −/− Natural mating
Atf7 −/− IVF
WT IVF
D
Relative Idi1 mRNA level
4
3
2
1
0
***
*
WT Natural mating
Atf7 −/− Natural mating
Atf7 −/− IVF
WT IVF
E
Oocyte
Sperm
Zygote
2-cell embryo
ICR female mice
Liver
stress during in vitro cultivation
H3K9me3
ATF7
ATF7
P
H3K9me3
H3K9me3

Acknowledgements

When I completed this doctoral thesis, I realized that I have been studying in Japan for nearly five years. I got the help and support from people around me since my first day as a member of Ph.D. program in Human Biology. It would be impossible for me to complete this doctoral program without the support from faculty, staff and students in this program.

Above all, I wish to express the sincerest appreciation to my supervisor Prof. Ishii for his guidance and support on my research project. I am grateful to him for his patience and kindness. I must thank him because he has always encouraged me to think independently and discussed with me about my ideas. More importantly, he shown me how to conduct research in a logical way. The training received from his guidance will benefit my entire scientific career in future.

I would like to thank all of members of Molecular Genetics Laboratory who gave me the suggestions on my project and offered help to my life. Specially, I would like to thank the members studying on the function of ATF7 in our laboratory, Dr. Meakawa, Dr. Yoshida and Dr. Liu, for their suggestions on experiments. I also want to thank Drs. Wakana and Furuse, for their support on animal experiments.

Thanks to the members of my dissertation committee, particularly to Profs. Takahashi and P. ten Dijke for their suggestions on my research. And I would to thank all of friends, classmates and staff in University of Tsukuba who helped me.

Last but not least, special thanks to my wife, my parents and my son. I really appreciate your support and encouragement to me. All of you are the reason why I wish to became stronger.